APPENDICES AVAILABLE ON THE HEI WEBSITE

Research Report 196

Developing Multipollutant Exposure Indicators of Traffic Pollution: The Dorm Room Inhalation to Vehicle Emissions (DRIVE) Study

Jeremy A. Sarnat et al.

Appendix A: Sampling Instrumentation and QA/QC Protocol
Appendix B: Measurement Details
Appendix C: Low-Cost Sensors
Appendix D: RLINE Calibration
Appendix E: Personal Exposures: Matching by Sampling Week
Appendix F: Metabolomics Analysis

These Appendices were reviewed solely for spelling, grammar, and cross-references to the main text. They have not been formatted or fully edited by HEI. This document was reviewed by the HEI Review Committee.

Correspondence may be addressed to Dr. Jeremy Sarnat, Emory University Rollins School of Public Health, 1518 Clifton Rd., Atlanta, GA 30322; e-mail: *jsarnat@emory.edu*.

Although this document was produced with partial funding by the United States Environmental Protection Agency under Assistance Award CR–83467701 to the Health Effects Institute, it has not been subjected to the Agency's peer and administrative review and therefore may not necessarily reflect the views of the Agency, and no official endorsement by it should be inferred. The contents of this document also have not been reviewed by private party institutions, including those that support the Health Effects Institute; therefore, it may not reflect the views or policies of these parties, and no endorsement by them should be inferred.

Appendix A: Sampling Instrumentation and QA/QC Protocol

The near-roadway stationary site collected continuous outdoor measurements for a large number of pollutants and meteorological variables, including BC, CO, O_3, NO_x, and direct NO_2. Direct NO_2 is a measurement approach (cavity attenuated phase shift technique) that measures NO_2 directly, not as the difference between NO_x and NO. An aerosol chemical speciation monitor also ran continuously, measuring both particle mass loading and some aerosol components. A meteorological station continuously collected wind speed and wind direction, temperature and relative humidity (RH), and precipitation. Additionally, quartz and Teflon filters collected $PM_{2.5}$ in 48-hour increments (Monday–Wednesday and Wednesday–Friday) for EC and OC. EC and OC were measured using a Lab OC–EC Aerosol Analyzer from Sunset Laboratory using the IMPROVE protocol. $PM_{2.5}$ mass and BC concentration were found using gravimetric and reflectance techniques. The filters were used to measure ROS using a fast DTT assay.

The near dorm and far dorm sites sampled continuously for CO, NO_x, particle count, BC, and $PM_{2.5}$ mass concentration using an optical particle counter. The continuous samplers alternated sampling indoor and outdoor air using a 15-minute timer and three-way valves. Filter-based measurements on quartz and Teflon were also collected. The RFT site in the Ford Environmental Science and Technology building served as a long-term continuous monitoring site, continuously monitoring NO_x, CO, O_3, $PM_{2.5}$, BC, and $PM_{2.5}$ particle mass using a TEOM, and meteorological parameters. Quartz and Teflon filters collected $PM_{2.5}$ in 48-hour increments, similar to the other sites. In addition, we used observations from the JST SEARCH monitor (Edgerton et al. 2005; Hansen et al. 2006) and the recently installed near-road monitor, also located on the GIT campus.

Further, we followed 54 college students living in the dormitories during the sampling period for personal exposure monitor sampling and biomonitoring, which included saliva and blood sampling. The personal monitor sampling included continuous $PM_{2.5}$ and 48-hour integrated NO_2 measurements as well as GPS tracking to determine exposure and behavioral differences between the participants living in the two dorms.

Table A.1 summarizes the completeness of data for the continuous instrumentation and integrated measurements at each sampling location and for the personal monitoring.

Table A.1. Instrumentation Used at Each Sampling Site and Completeness of Each Data Parameter

Sampling Site	Distance from Highway	BC	CO	NO-NO_2-NO_x	Direct NO_2		ACSM	Particle Count	Filter for EC/OC/DTT	$PM_{2.5}$ Mass	Weather Data
RDS	0.1 km	X/O	X	X	X	X	X	--	O	O	X
		79%/78%	76%	93%	100%	99%			73%	78%	61%
RFT	0.5 km	X/O	X	X	--	--	--	--	O	X/O	X
		90%/67%	70%	89%					69%	79%/67%	99%
NDO	0.2 km	X/O	X	X	O	--	--	X	O	O	--
		34%/94%	77%	82%	96%			35%	94%	94%	
FDO	1.2 km	X/O	X	X	O	--	--	X	O	O	--
		34%/100%	66%	65%	98%			21%	94%	100%	
EPD	0.05 km	X	X	X	--	X	--	--	--	--	--
		39%	98%	97%		98%					
JST	2.3 km	X	X	X	--	X	--	--	--	--	X
		100%	92%	92%		98%					96%
Personal	---	O	--	--	O	--	--	--	--	X/O	--
		86%			66%					79%/86%	

ACSM = aerosol chemical speciation monitor; X = continuous, completeness based on ratio of hours with valid data and total hours from Sept. 8 to Jan. 5 (n = 2880 hours); O = integrated 48-hour, completeness based on ratio of 48-hr periods with valid data and target number of 48-hr periods from Sept. 8 to Jan. 5 (n = 26 periods); -- = parameter not measured.

The QA–QC protocol addressed corrections and calibrations adopted to address temporal misalignment, data exclusion, and other instrument-specific data processing considerations. The protocol included using data quality parameters for each pollutant, where available. All instruments used to measure continuous pollutant concentrations were refurbished and calibrated before field sampling. Instrument collocations were conducted for continuous NO_2/NO_x, CO, and integrated $PM_{2.5}$ mass and reflectance over a multi-day period, both before and after field sampling to assess method precision and potential instrument offset. In addition, redundant instrumentation was deployed to provide an additional means of assessing data quality when possible.

NO_x (Continuous) Protocol

Data files were regularly downloaded and concatenated into as few Microsoft Excel sheets as possible. The first step was to verify the time alignment between instruments by adjusting values to Eastern Standard Time as necessary and correcting for temporal misalignment or temporal drift among the instruments. In addition, the 15-minute value used to alternate between indoor and outdoor sampling drifted by about 10–15 seconds per day. By observing a single hour for each day of the study, the moment the valve switched could be precisely identified. This observed daily valve

switch time was applied to the other times throughout the day that the valve switched. By calculating a new valve switch time, the data could then be divided into standard 15-minute periods in order to divide the data between indoor and outdoor data. The second step was to apply the NO calibration curves that were generated at several points throughout the study period to capture any measurement drift that occurred in the instrument using a time-weighted average method. The third step was to reduce the data frequency from less than a minute to hourly, daily, and total averages. The quarterly average was also reported for the sites that were sampling indoor and outdoor concentrations. The fourth step was to adjust the data based on the collocation data that was collected before and after the study in order to determine the offset correction that was necessary for the instruments to be directly compared.

In order to correct the NO_2 (i.e., the difference between the NO and NO_x direct measurements), the above steps were also followed, including the use of the NO calibration curve. After the sampling period concluded, the instruments were collocated with the direct NO_2 measurement instrument for further correction. The NO_x concentration reported was calculated based on the sum of the corrected NO and NO_2 concentrations.

Direct NO_2 (Continuous) Protocol

Data files were opened in Microsoft Excel so that the daily baseline calibration period could be removed. The daily calibration was necessary to quantify any drift that occurred in the instrument and took about 5 minutes a day. The measurement data were then calibrated using a time-weighted adjustment between each baseline reading. The data frequency was then reduced to 15-minute, hourly, and daily averages.

CO (Continuous) Protocol

Along with the voltage data that were later converted to concentration data, a separate file was generated to designate when the instrument was measuring ambient air or zero air. Both files were opened as CSV files and then imported into R version 3.0.1 so that the difference between the zero air measurement and the ambient air measurement could be calculated for an accurate reading of the CO concentration. Because the CO instruments were on the same valve as the NO_x instruments, a similar method was used to adjust the time alignment of the instruments and account for the drift in the valve first. The second step was to calculate the difference between the voltage data. The data switched between sample and zero air every 7.5 minutes, but there was a varying period of time needed for the voltage to transition and stabilize depending on the concentration. Different time lengths were assessed to determine which successfully avoided issues with overlap between sample and blank measurements while providing stable estimates of the sample and blank voltage readings. The final 4 minutes of each 7.5-minute measurement were used in the difference calculation. Because the calibration curves converting from voltage to concentration were linear, the difference could be calculated first; then the calibration could be applied using a time-weighted average method. The third step was to reduce the data frequency from less than a minute to hourly, daily, and total averages.

Condensation Particle Counter (Continuous) Protocol

The condensation particle counter (CPC) instruments collected 1-minute data alternating between indoor and outdoor sampling, so the time alignment and valve drift adjustments used for the NO_x instruments were also necessary for the two CPC instruments before the data were averaged.

Optical Particle Counter (Continuous) Protocol

Although the optical particle counter (OPC) was on the 15-minute valve with the NO_x and CO instruments, because the clock was reset every 48 hours to standard time, no time alignment adjustments were necessary. Further, only the middle 10 minutes of the 15-minute data period were used, to eliminate the valve drift issue. The size-resolved number concentration was converted to a nominal $PM_{2.5}$ volume concentration by assuming that all particles recorded in each OPC channel were spheres with a diameter equal to the log-average midpoint of the corresponding channel so that a total particle volume was calculated for each channel. The $PM_{2.5}$ volume was calculated by summing across the 15 channels with an optical diameter less than 2.5 µm. Finally, an average indoor and outdoor volume concentration was calculated for each 48-hour session. The 48-hour sampling periods for the OPC instruments were aligned with filter sample collection. During each 48-hour sampling period, the indoor and outdoor $PM_{2.5}$ mass concentrations were independently measured using collocated filter samples. These measurements were used to calculate a "synthetic density" in units of $g \cdot cm^{-3}$ by dividing the gravimetric mass concentration by calculated volume concentration. This was repeated both indoors and outdoors at each location for each 48-hour sample period. The synthetic density was then applied to each of the corresponding 15-minute indoor or outdoor samples to calculate the $PM_{2.5}$ mass concentration with 15-minute time resolution.

$PM_{2.5}$ Mass (Continuous) and $PM_{2.5}$ BC Protocols

The ambient 5-minute data were corrected with the average of the blank measurements collected when a HEPA filter was placed on the instrument inlet. Only the BC data measured from the Aethalometer were corrected according to the procedure described in "A Simple Procedure for Correcting Loading Effects of Aethalometer Data" (Virkkula et al. 2007).

References for Appendix A

Edgerton ES, Hartsell BE, Saylor RD, Jansen JJ, Hansen DA, Hidy GM. 2005. The Southeastern Aerosol Research and Characterization Study: Part II. Filter-based measurements of fine and coarse particulate matter mass and composition. J Air Waste Manage Assoc 55:1527–1542.

Hansen DA, Edgerton E, Hartsell B, Jansen J, Burge H, Koutrakis P, et al. 2006. Air quality measurements for the aerosol research and inhalation epidemiology study. J Air Waste Manage Assoc 56:1445–1458.

Virkkula A, Mäkelä T, Hillamo R, Yli-Tuomi T, Hirsikko A, Hämeri K, Koponen IK. 2007. A simple procedure for correcting loading effects of aethalometer data. J Air Waste Manage Assoc 57(10):1214–1222.

Appendix B: Measurement Details

Table B.1 contains detailed data on the observations and modeled pollutant-related quantities made as part of the DRIVE study, excluding the results from the multisensory units, which were run for shorter periods. Not all pollutants were measured at all the sites (see Table 1 of main report). Figure B.1 provides graphical depictions of the observations, including all outliers that were removed from Figure 3 in the main report. Including the outliers in Figure B.1 and showing the time series in Figure B.2 highlights the extreme hourly and daily concentrations, respectively, that were measured during the study. Table B.2 shows the results of the regression analysis between the single pollutant measurements and the IMSI at each sampling location. For comparison, Figure B.3 shows the normalized diurnal variations of the RDS observations of BC, CO, NO_x, NO_2, IMSI, O_3, and on-road traffic count. Figure B.4 is the wind rose for the RDS meteorology monitor and Figure B.5 shows the rate of emissions based on vehicle speed.

Table B.1. **Summary of Observational and Modeled Data from September 8, 2014, to January 5, 2015**
(RDS-CAPS [cavity attentuated phase shift] = RDS CAPS direct NO_2).

		EPD	RDS	NDO	NDI	RFT	FDO	FDI	JST	RDS-CAPS
BC ($\mu g/m^3$)	N	1113	2280	978	978	2592	925	1061	2875	-
	Mean	1.69	1.60	0.94	0.77	0.90	0.80	0.61	0.82	-
	SD	1.25	1.33	1.59	1.42	0.79	1.67	1.20	0.85	-
	Q1	0.86	0.71	0.40	0.33	0.41	0.27	0.20	0.33	-
	Median	1.39	1.19	0.84	0.63	0.67	0.61	0.48	0.51	-
	Q3	2.17	2.16	1.47	1.09	1.10	1.26	1.01	0.95	-
NO (ppb)	N	2798	2666	2357	2356	2564	1883	1883	2655	-
	Mean	37.95	20.93	15.95	7.35	4.15	11.78	3.86	13.16	-
	SD	29.11	23.47	26.01	14.95	11.23	28.35	18.72	30.08	-
	Q1	16.60	5.64	4.54	3.20	-0.55	0.37	-2.86	0.65	-
	Median	31.30	12.76	8.52	4.85	0.78	4.04	1.47	2.03	-
	Q3	50.90	28.58	15.85	7.25	3.68	11.08	3.70	8.18	-
NO_2	N	2798	2666	2357	2356	2564	1883	1883	2654	2878

(ppb)	Mean	19.46	29.09	23.29	26.86	20.78	21.25	25.77	13.01	21.95
	SD	8.57	15.55	13.01	20.63	10.38	6.93	12.18	9.82	11.70
	Q1	12.90	16.96	13.09	13.91	12.60	15.59	16.95	5.32	13.33
	Median	18.90	26.63	20.48	19.86	17.37	19.15	21.16	9.97	20.42
	Q3	24.60	37.93	30.98	31.67	27.35	25.75	31.11	18.75	28.53
NO_x (ppb)	N	2798	2666	2357	2356	2564	1883	1883	2627	-
	Mean	57.32	50.03	39.24	34.21	24.94	33.03	29.64	27.65	-
	SD	34.35	34.45	35.00	32.26	18.31	32.37	27.63	37.06	-
	Q1	32.10	24.82	18.98	18.12	12.58	16.24	15.89	7.81	-
	Median	51.10	41.81	29.05	24.58	18.38	22.51	21.36	13.59	-
	Q3	74.30	66.55	46.53	37.43	31.25	36.97	33.87	29.35	-
CO (ppb)	N	2816	2178	2226	2223	2017	1914	1874	2648	-
	Mean	623.97	424.90	343.77	321.12	275.22	204.36	201.82	268.33	-
	SD	337.72	209.78	169.68	179.52	151.23	191.22	183.58	197.41	-
	Q1	400.00	277.54	231.70	204.11	191.04	90.91	93.26	157.26	-
	Median	600.00	372.29	297.82	265.42	232.25	155.84	156.80	205.69	-
	Q3	800.00	515.28	413.31	388.20	301.70	238.40	236.73	282.29	-
$PM_{2.5}$ Mass TEOM ($\mu g/m^3$)	N	2448	-	-	-	-	-	-	2531	-
	Mean	10.44	-	-	-	-	-	-	9.02	-
	SD	5.24	-	-	-	-	-	-	5.27	-
	Q1	6.70	-	-	-	-	-	-	5.29	-
	Median	9.72	-	-	-	-	-	-	7.77	-
	Q3	13.40	-	-	-	-	-	-	11.64	-

O_3 (ppb)	N	2820	2850	-	-	-	-	-	2833	-
	Mean	14.73	18.15	-	-	-	-	-	19.50	-
	SD	12.99	11.70	-	-	-	-	-	13.83	-
	Q1	2.00	8.51	-	-	-	-	-	7.26	-
	Median	12.00	16.91	-	-	-	-	-	18.77	-
	Q3	23.00	25.47	-	-	-	-	-	28.89	-
OPC ($1\ 1000^{-1}\ m^{-3}$)	N	-	-	1019	1021	-	610	612	-	-
	Mean	-	-	10.91	8.92	-	10.70	9.74	-	-
	SD	-	-	6.02	5.68	-	6.71	6.00	-	-
	Q1	-	-	6.25	5.01	-	5.64	5.49	-	-
	Median	-	-	9.90	7.53	-	9.20	9.09	-	-
	Q3	-	-	14.61	11.48	-	14.36	13.20	-	-
IMSI	N	890	1583	856	852	1890	708	712	2441	-
	Mean	1.82	1.64	1.41	1.27	1.46	1.00	1.07	1.09	-
	SD	1.03	0.87	0.98	0.98	0.97	0.93	0.98	1.00	-
	Q1	1.04	1.00	0.81	0.71	0.86	0.50	0.24	0.53	-
	Median	1.67	1.43	1.16	0.99	1.13	0.75	0.81	0.72	-
	Q3	2.35	2.07	1.72	0.48	1.71	1.17	1.23	1.18	-
RLINE $PM_{2.5}$ ($\mu g/m^3$)	N	2906	2906	2906	-	2906	2906	-	2906	-
	Mean	1.09	1.25	0.90	-	0.53	0.52	-	0.38	-
	SD	2.81	2.91	2.38	-	1.64	1.47	-	1.26	-
	Q1	0.10	0.16	0.08	-	0.03	0.07	-	0.04	-
	Median	0.27	0.39	0.22	-	0.09	0.13	-	0.08	-
	Q3	0.87	1.05	0.60	-	0.30	0.33	-	0.22	-
RLINE CO (ppb)	N	2906	2906	2906	-	2906	2906	-	2906	-
	Mean	45.16	51.53	37.09	-	22.90	22.35	-	16.90	-
	SD	112.47	116.06	95.40	-	67.80	61.50	-	53.05	-

	Q1	4.59	6.68	3.71	-	1.55	3.05	-	1.79	-
	Median	11.82	16.89	9.23	-	4.05	5.65	-	3.44	-
	Q3	36.00	44.14	25.22	-	12.68	14.08	-	9.53	-
RLINE NO_x (ppb)	N	2906	2906	2906	-	2906	2906	-	2906	-
	Mean	7.52	8.58	6.13	-	3.75	3.67	-	2.78	-
	SD	18.82	19.43	15.85	-	11.20	10.16	-	8.81	-
	Q1	0.76	1.11	0.61	-	0.25	0.50	-	0.29	-
	Median	1.94	2.80	1.51	-	0.66	0.91	-	0.56	-
	Q3	6.02	7.33	4.14	-	2.08	2.32	-	1.59	-

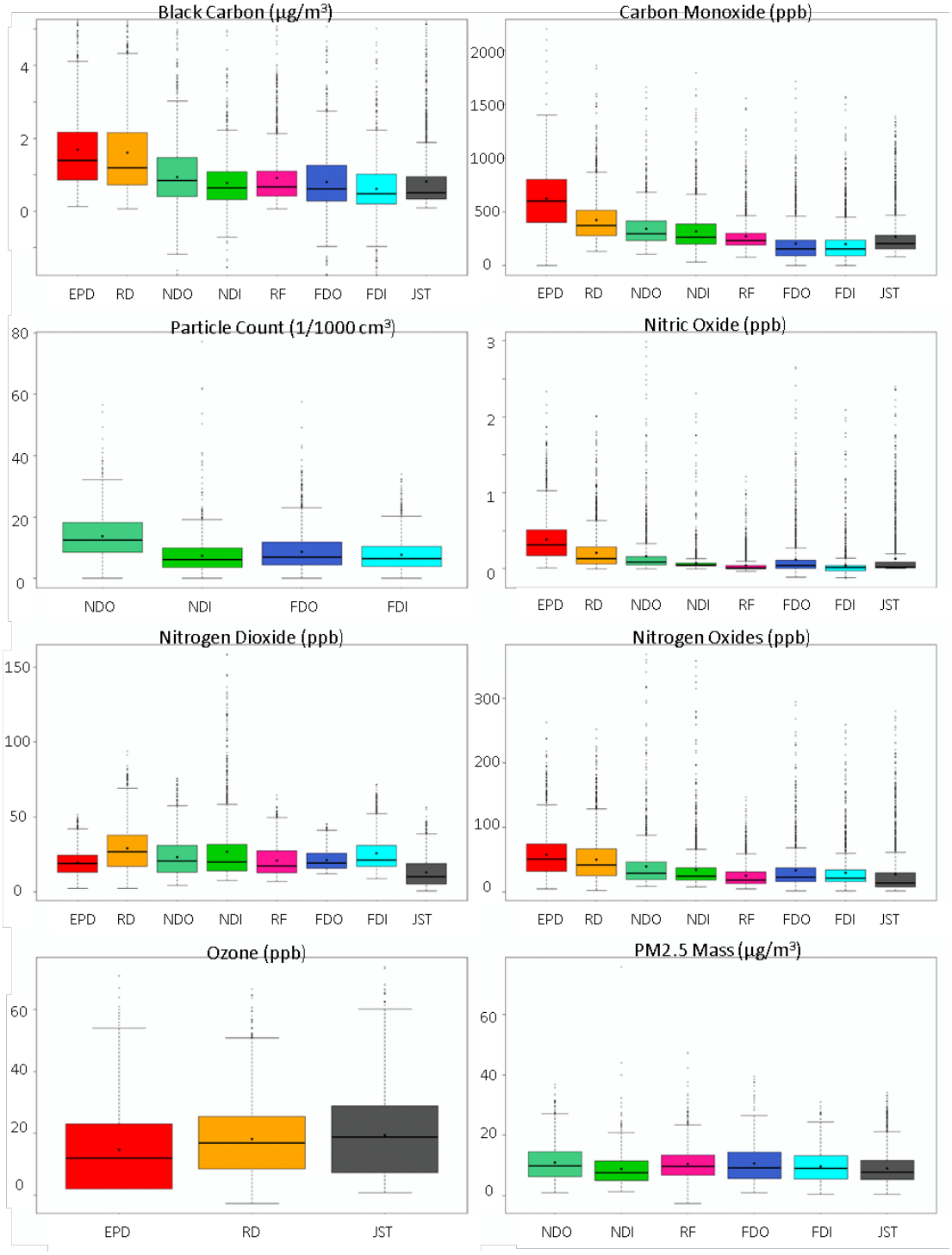

Figure B.1. Hourly mean concentration data including all outliers outside the interquartile range for BC, CO, CPC, NO, NO_2, NO_x, O_3, and $PM_{2.5}$ from September 8, 2014, to January 5, 2015, at the sampling sites ordered by increasing distance from the highway source: (EPD) Georgia Department of Natural Resources Near-road Network Monitor [5 m], (RDS) Near-roadway stationary site [10 m], (NDO) Near Dorm outside [20 m], (NDI) Near Dorm inside [20 m], (RFT) Rooftop lab [500 m], (FDO) Far Dorm outside [1.4 km], (FDI) Far Dorm inside [1.4 km], (JST) Urban background [2 km].

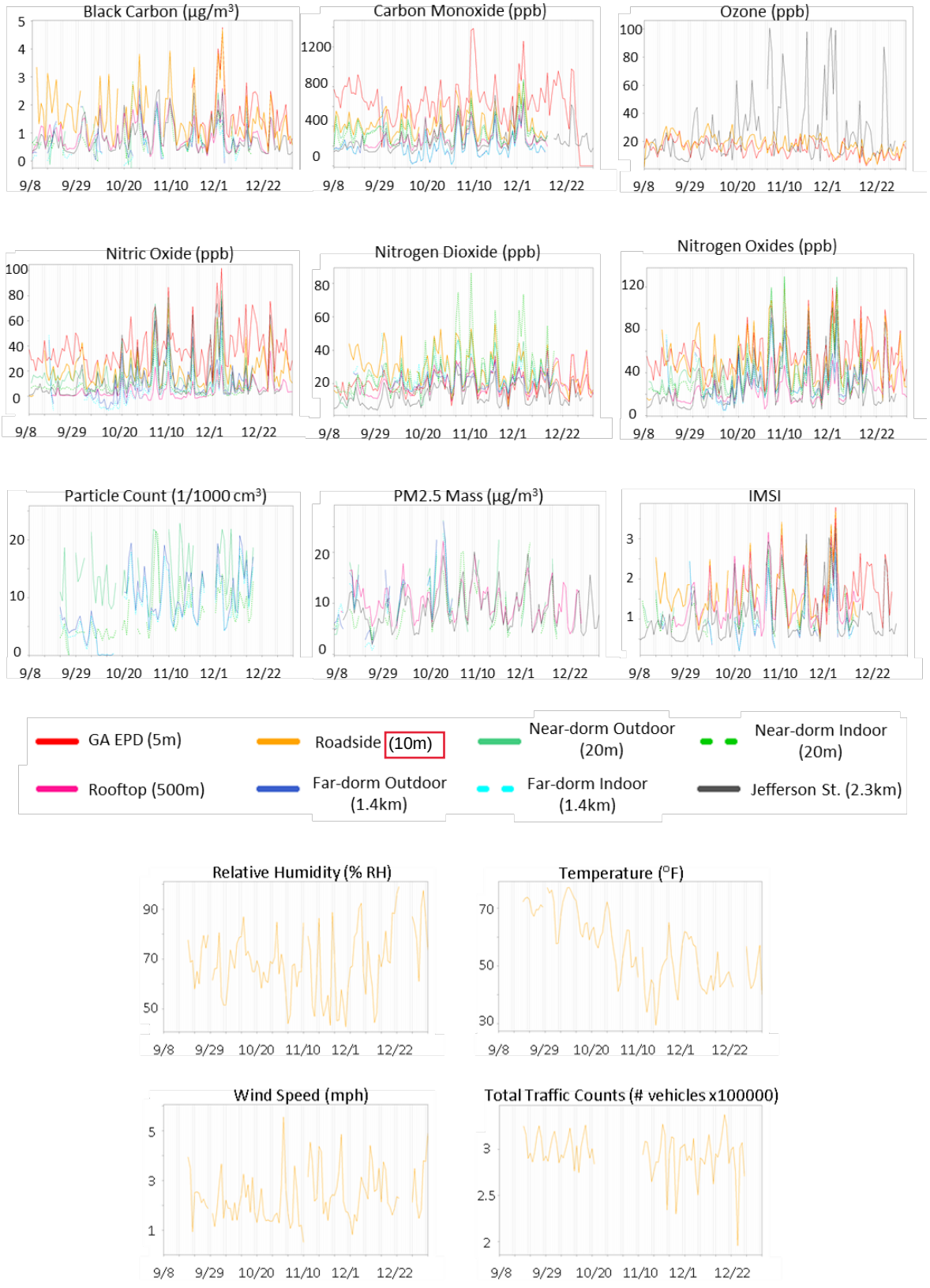

Figure B.2. Time series plots for daily BC, CO, CPC, NO, NO_2, NO_x, O_3, $PM_{2.5}$, IMSI, RH, wind speed, temperature, and total traffic counts from September 8, 2014, to January 5, 2015.

Table B.2. Regression Analysis (R^2) Between IMSI and Measurements

	EPD (N = 890)	RSD (N = 1583)	NDO (N = 856)	NDI (N = 852)	RFT (N = 1890)	FDO (N = 708)	FDI (N = 712)	JST (N = 2443)
CO	0.90	0.68	0.83	0.83	0.89	0.81	0.850	0.93
NO_x	0.96	0.84	0.78	0.80	0.90	0.78	0.81	0.93
BC	0.89	0.77	0.43	0.39	0.92	0.44	0.52	0.91
$PM_{2.5}$	--	--	--	--	0.44	--	--	0.59

(A)

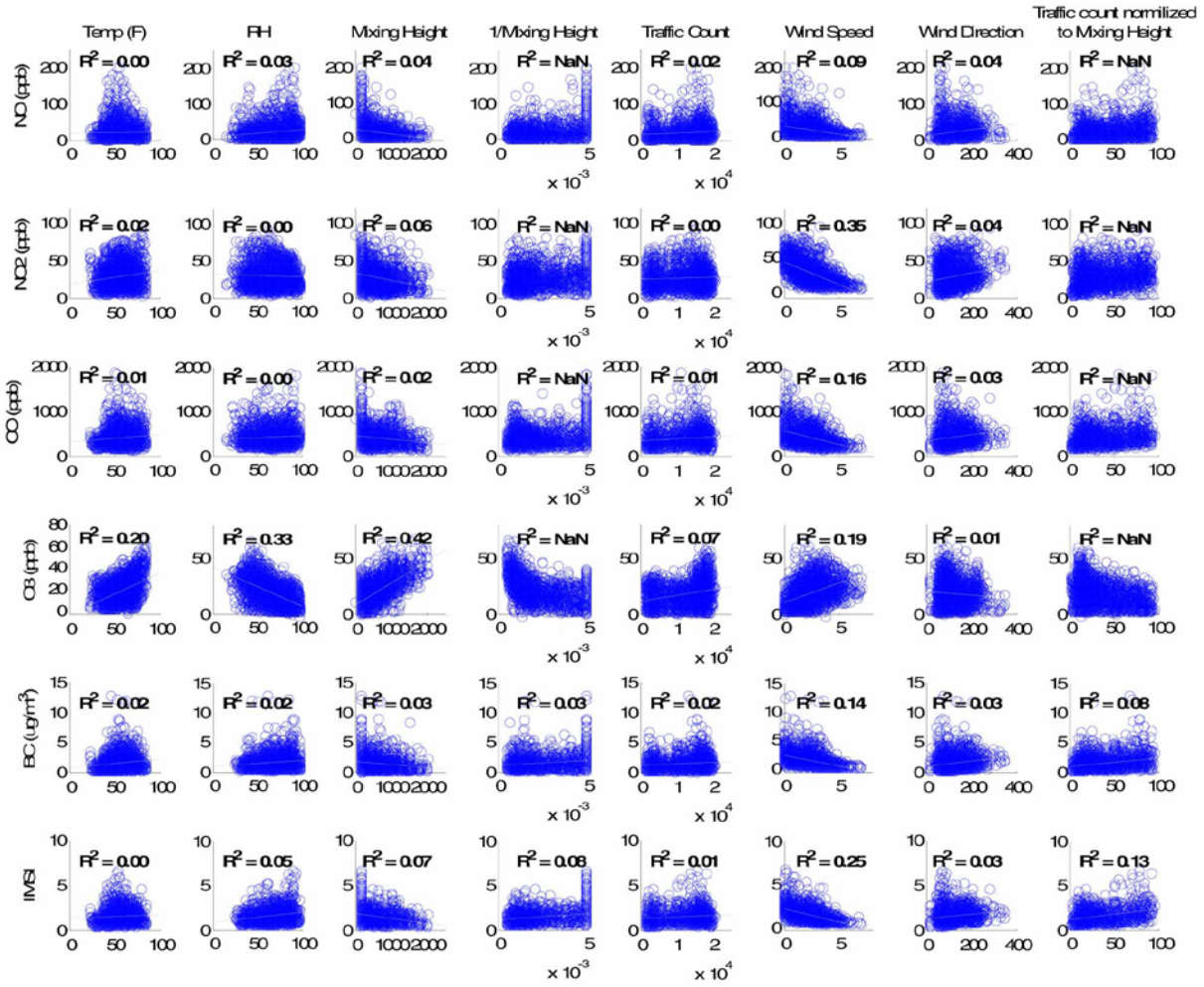
Temp (F)
RH
Mixing Height
1/Mixing Height
Traffic Count
Wind Speed
Wind Direction
Traffic count normilized to Mixing Height
NO (ppb)
NO2 (ppb)
CO (ppb)
O3 (ppb)
BC (ug/m3)
IMSI
R2 = 0.00
R2 = 0.03
R2 = 0.04
R2 = NaN
R2 = 0.02
R2 = 0.09
R2 = 0.04
R2 = NaN
R2 = 0.02
R2 = 0.00
R2 = 0.06
R2 = NaN
R2 = 0.00
R2 = 0.35
R2 = 0.04
R2 = NaN
R2 = 0.01
R2 = 0.00
R2 = 0.02
R2 = NaN
R2 = 0.01
R2 = 0.16
R2 = 0.03
R2 = NaN
R2 = 0.20
R2 = 0.33
R2 = 0.42
R2 = NaN
R2 = 0.07
R2 = 0.19
R2 = 0.01
R2 = NaN
R2 = 0.02
R2 = 0.02
R2 = 0.03
R2 = 0.03
R2 = 0.02
R2 = 0.14
R2 = 0.03
R2 = 0.08
R2 = 0.00
R2 = 0.05
R2 = 0.07
R2 = 0.08
R2 = 0.01
R2 = 0.25
R2 = 0.03
R2 = 0.13
x 10-3
x 10^4

(B)

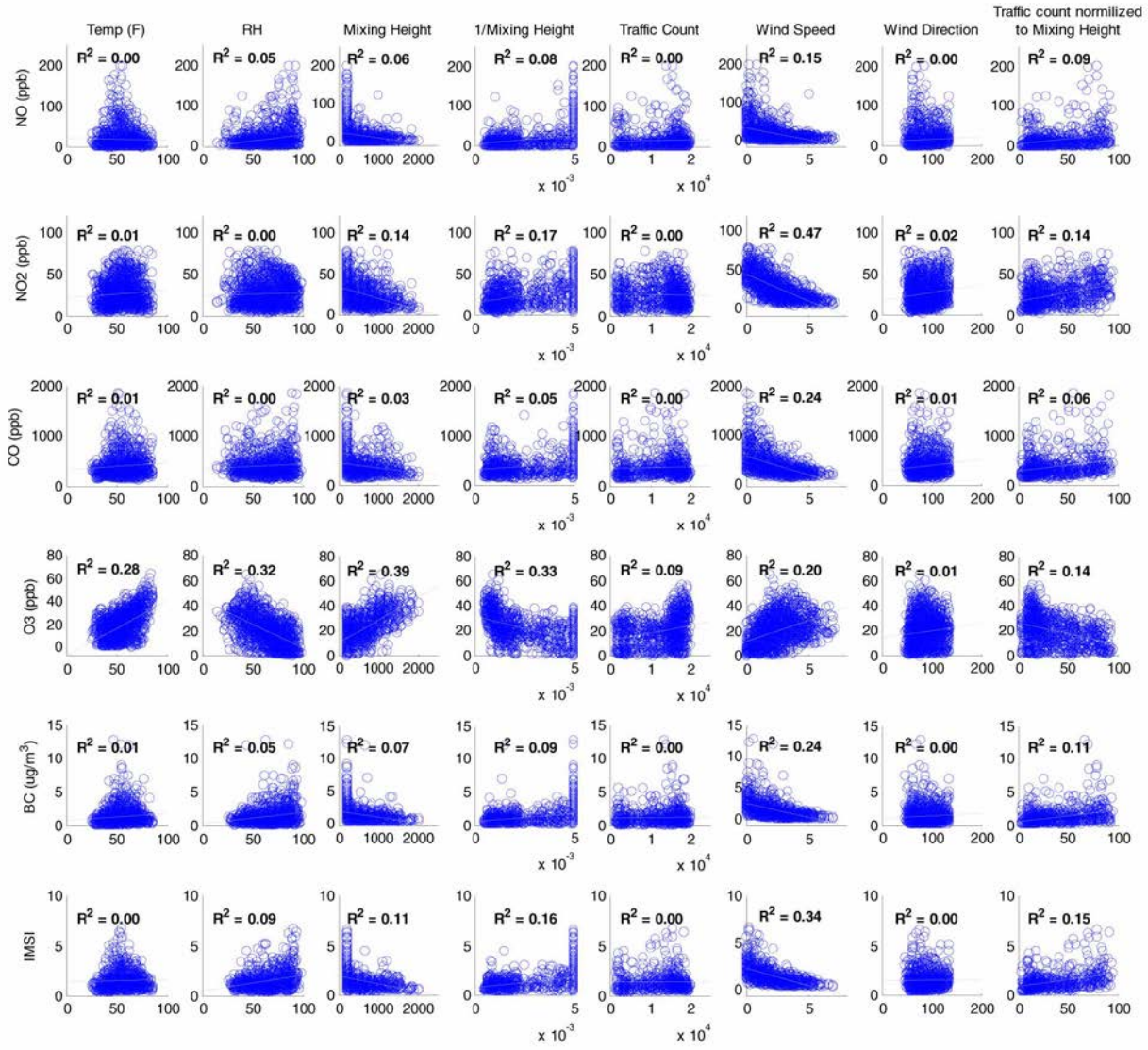

Figure B.3. Scatterplots showing correlations between hourly RDS pollutant measurements and pollutant indicators from September 1, 2014, to December 31, 2014, at (A) all hours and (B) only the hours when wind direction was from the east.

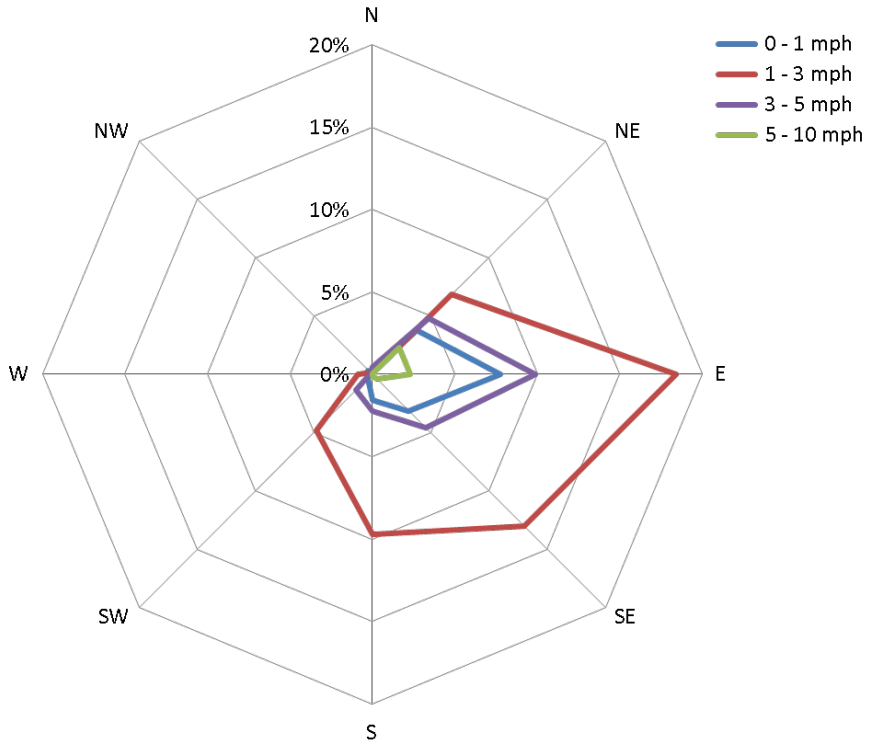

Figure B.4. Wind rose for RDS meteorology station for September 8, 2014, to January 5, 2015.

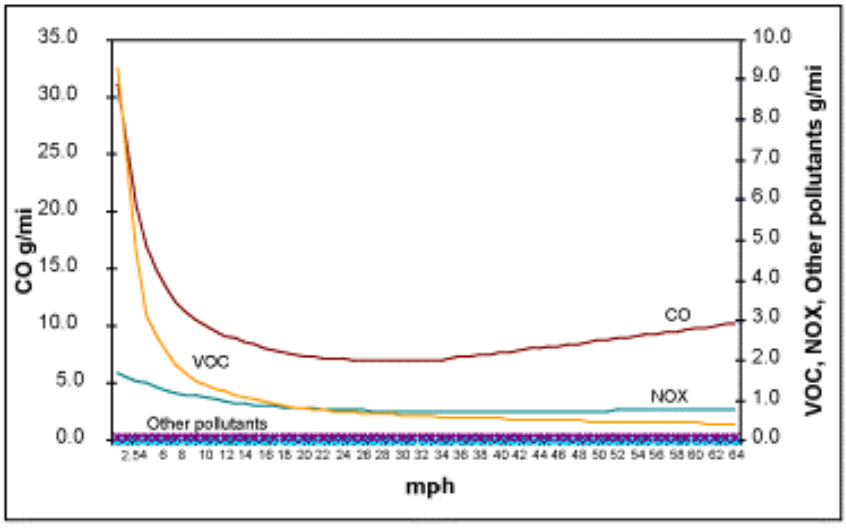

Figure B.5. Emissions factors by speed for light-duty vehicles and trucks (U.S. DOT).

Table B.3 shows the effects of distance from each monitoring site to the roadside, modified by several factors, including temporal, meteorological, and traffic count factors (same as in Table 2). The results and interpretations for time of day analyses are supported by results from other factors, particularly those for wind speed and traffic counts. These factors were modeled as continuous modifiers. The table shows the magnitude and significance of just the interaction term for these modifiers; the values show how the spatial decay was "enhanced" or "attenuated" by the factor. For example, interaction terms for wind speed were consistently less than 1 for all pollutants, indicating that hours with higher wind speed had a larger negative distance effect and thus a stronger spatial decay gradient. For traffic counts, interaction terms with "distance" were less than 1 for CO and IMSI, indicating that during hours with higher traffic counts, the spatial gradient was more apparent. In this analysis of modeling ratios, it was also of interest to compare across pollutants. For example, "distance" effects were generally smallest for NO compared with other pollutants. These results suggest that NO concentrations experience a stronger spatial gradient compared with those of other pollutants and are consistent with atmospheric chemistry resulting in the rapid oxidation of NO to other NO_x species (e.g., NO_2).

Table B.3. Associations Between Distance from the RDS Site (per 50 m) and Outdoor Pollutant Concentrations: Effect Modification by Various Factors^

	BC	CO	NO	NO_2	IMSI
Categorical Factors[#]					
Time Period of the Day					
Evening Rush Hour (4pm-7pm)	0.991[&,**]	0.980[&,**]	0.954[&,**]	0.988[&,**]	0.992[&,**]
Late Evening (8pm-11pm)	0.992	0.983*	0.967**	0.991**	0.993
Midday (10am-3pm)	0.987**	0.975**	0.960*	0.977**	0.985**
Midnight & Early Morning (12am-5am)	0.993*	0.986**	0.971**	0.991**	0.994
Morning Rush Hour (6am-9am)	0.991	0.984*	0.976**	0.988	0.990
Wind Direction (relative to RDS site)					
Westerly	0.990[&,**]	0.980[&,**]	0.956[&,**]	0.977[&,**]	0.987[&,**]
Northerly	0.998*	0.989**	0.990**	0.994**	0.996**
Easterly (toward GIT campus)	0.992	0.984*	0.971**	0.990**	0.992**
Southerly	0.987	0.979	0.958	0.983**	0.988

Date of Week					
Weekday	0.992[&,**]	0.982[&,**]	0.967[&,**]	0.988[&,**]	0.992[&,**]
Weekend	0.989*	0.982	0.960**	0.986**	0.989**
Continuous Factors[##]					
Temperature (F)	1.000	1.000**	1.000**	1.000**	1.000**
Relative Humidity (%)	1.000**	1.000*	1.000**	1.000**	1.000*
Wind Speed (mph)	0.999**	0.996**	0.993**	0.998**	0.997**
Traffic Counts (per 1,000)	1.000**	0.999**	1.000	1.000**	0.995**

^ Modification assessed using distance*factor product terms, with each factor tested in different models; [#] Categorical factor results show the effects of distance (per 50 m from roadway) on pollutant concentrations for each level of the factor; [##] Continuous factor results show the interaction term parameter estimate; [&] Reference category showing magnitude and significance of "distance" main effect (note: results for other levels of each category show the magnitude of the "distance" effect and whether the effect is significantly different from the reference category); ** *P* value < 0.001; * *P* value < 0.05.

Fine Particulate Matter Oxidative Potential

The second part of Appendix B provides additional details about the FPMOP indicator. Table B.3 shows the association between the RDS site and the other outdoor sites. Table B.4 and Table B.5 show details of the regression analysis using Pearson's *r* between $OP^{WS\text{-}DTT}$ volume and mass normalized, respectively, at various sites and the pollutant measurements. Details about the metals analysis are also included in this appendix. Table B.6 provides the mean ratios of simultaneous measurements from the EPD site and the RDS site. Table B.7 shows the correlations using Pearson's *r* between $FPMOP^{DTT}$ and $PM_{2.5}$ species components at the EPD and RFT sites.

Table B.4. Regression Analysis (Pearson's *r*) Between FPMOP$^{WS\text{-}DTT}$/m^3 and PM Mass, OC, EC, CO, NO_x, BC, and IMSI at Various Sampling Sites†

	RDS (N = 18)	NDO (N = 20)	NDI (N = 21)	RFT (N = 16)	FDO (N = 17)	FDI (N = 17)
$PM_{2.5}$ mass	**0.87**	0.58	**0.81**	0.67**	**0.77**	0.68
OC	**0.88**	**0.91**	**0.86**	**0.91**	**0.90**	**0.80**
EC	**0.77**	0.69	**0.85**	**0.85**	**0.91**	**0.91**
CO	0.56*	**0.71**	0.60	**0.76**	**0.75**	0.59
NO_x	0.46*	**0.79**	**0.76**	**0.82**	**0.76**	**0.76**
BC	0.60	0.56	**0.75**	**0.74**	**0.83**	**0.77**
IMSI	0.41**	**0.70**	0.65	**0.78**	**0.72**	0.60*

Note: $r > 0.70$ are boldface.

†Online measurements were averaged to the filter sampling times. All data are based on filter analysis, with the exception of CO, NO_x, BC, and IMSI. Correlations significant at the 0.01 level ($P < 0.01$) are without superscript; * = $P < 0.05$; ** = correlation is not significant.

Table B.5. Regression Analysis (Pearson's *r*) Between FPMOP$^{WS\text{-}DTT}$/µg at Various Sites and OC or EC Content in Unit PM Mass†

	RDS (N = 15)	NDO (N = 22)	NDI (N = 21)	RFT (N = 8)	FDO (N = 22)	FDI (N = 24)
OC	0.39**	**0.88**	0.58	0.82*	**0.86**	**0.90**
EC	0.32**	0.59	0.43*	**0.84**	**0.75**	**0.87**

Note: $r > 0.70$ are bold.

†All data are based on filter analysis. Correlations significant at the 0.01 level ($P < 0.01$) are without superscript; * = $P < 0.05$; ** = correlation is not significant.

Metals Analysis Method

For determining total metals, samples were digested in 1:3 HNO_3:HCl solution, diluted in deionized water, then filtered with 0.45-µm syringe filters. For measuring water-soluble metals, filters were sonicated in deionized water for 0.5 hr with an ultrasonic cleanser (VWR International LLC, West Chester, PA, USA). After sonication, the extracts were filtered using 0.45-µm syringe filters; then HNO_3 was added to produce a final concentration of 2%. A set of metal standards were treated with the same procedures as the samples to establish filter mass concentrations from the inductively coupled mass spectrometry responses. The R^2 of the standard calibration curves ranged from 0.943 to 0.999 (N = 8) for various metals. A 25-ppb internal standard of scandium was added to all samples and standards to monitor analytical drift.

Table B.6. Mean Ratios of Simultaneously Measured Metals and FPMOP between RFT and EPD sites for Water-Soluble and Total Components

		K	Mn	Fe	Cu	Zn	$FPMOP^{DTT}$
$\frac{WS\ conc._{RFT}}{WS\ conc._{EPD}}$	N	29	29	29	29	29	31
	Mean	0.80	0.42	0.43	0.90	0.49	0.98
	STD	0.25	0.14	0.10	0.45	0.22	0.12
$\frac{Total\ conc._{RFT}}{Total\ conc._{EPD}}$	N	29	29	29	29	-	32
	Mean	0.90	0.37	0.33	1.04	-	0.94
	STD	0.40	0.16	0.14	0.59	-	0.14
$\frac{(WS/Total)_{RFT}}{(WS/Total)_{EPD}}$	N	29	29	29	29	-	31
	Mean	0.96	1.25	1.50	0.94	-	1.05
	STD	0.40	0.66	0.65	0.21	-	0.18

Table B.7. Correlation matrix (Pearsons *r*) for various water-soluble and total components and $FPMOP^{DTT}$ at the EPD and RFT site.

	RD			WS						Total						W_in					
		OC	EC	$FPMOP^{DTT}$	K	Mn	Fe	Cu	Zn	$FPMOP^{DTT}$	K	Mn	Fe	Cu	Zn	$FPMOP^{DTT}$	K	Mn	Fe	Cu	Zn
	EC	**0.75**	1																		
WS	DTT	**0.83**	**0.79**	1																	
	K	**0.86**	0.68	0.67	1																
	Mn	**0.79**	0.63	0.43*	0.56	1															
	Fe	**0.8**	**0.8**	**0.88**	0.66	0.45*	1														
	Cu	0.64	**0.78**	0.54	**0.77**	0.36**	0.63	1													
	Zn	**0.78**	**0.79**	0.51*	0.68	**0.84**	**0.75**	**0.7**	1												
Total	DTT	**0.71**	0.68	0.56	0.6	0.56	0.49*	0.55	0.46*	1											
	K	**0.88**	**0.71**	0.69	**0.9**	0.65	**0.72**	0.51*	0.68	0.67	1										
	Mn	**0.86**	0.69	0.48*	0.53	**0.95**	0.56	0.56	**0.82**	0.66	0.61	1									
	Fe	**0.79**	**0.75**	0.57	0.55	**0.72**	**0.72**	**0.71**	**0.78**	0.66	0.6	**0.9**	1								
	Cu	0.66	**0.72**	0.40**	**0.78**	0.65	0.56	**0.93**	0.65	**0.72**	0.57	**0.79**	**0.84**	1							
	Zn	-0.59	-0.26**	-0.48*	-0.65	0.54	-0.47*	-0.33**	-0.31**	0.37**	-0.55	0.51	-0.29**	0.22**	1						
W_In	DTT	-0.34**	-0.37**	-0.51	-0.47*	-0.37**	-0.40*	-0.40*	-0.52	**0.84**	-0.43*	0.31**	-0.39*	0.43*	0.25**	1					
	K	0.6	0.47*	0.37**	0.40**	0.56	**0.73**	0.28**	0.55	0.47*	**0.7**	0.63	0.62	0.24*	-0.21**	-0.27**	1				
	Mn	**0.77**	**0.72**	0.42*	0.44*	**0.81**	0.62	0.65	**0.75**	0.67	0.49*	**0.95**	**0.96**	**0.82**	0.38**	0.31**	0.57	1			
	Fe	**0.74**	**0.71**	0.47*	0.49*	**0.71**	0.66	**0.7**	**0.78**	0.66	0.54	**0.9**	**0.998**	**0.84**	-0.26**	-0.36**	0.59	**0.97**	1		
	Cu	0.67	**0.73**	0.25**	**0.79**	0.65	0.56	**0.92**	0.68	**0.73**	0.59	**0.79**	**0.84**	**0.9996**	0.23**	0.44*	0.14**	**0.82**	**0.84**	1	
	Zn	-0.65	-0.47*	-0.51*	-0.69	0.31**	-0.58	-0.36**	-0.43**	0.23**	-0.6	-0.19**	-0.39*	-0.28**	**0.99**	0.22**	-0.22**	-0.21**	-0.35**	-0.29**	1

	GT			WS						Total					W_In				
		OC	EC	$FPMOP^{DTT}$	K	Mn	Fe	Cu	Zn	$FPMOP^{DTT}$	K	Mn	Fe	Cu	$FPMOP^{DTT}$	K	Mn	Fe	Cu
	EC	**0.83**	1																
WS	DTT	**0.79**	**0.84**	1															
	K	0.6	**0.88**	0.63	1														
	Mn	**0.86**	**0.7**	0.46*	0.54	1													
	Fe	**0.8**	**0.82**	0.49*	0.62	**0.82**	1												
	Cu	**0.7**	**0.78**	**0.77**	**0.71**	**0.72**	0.64	1											
	Zn	0.63	0.52*	0.44*	0.51	**0.89**	0.65	**0.72**	1										
Total	DTT	0.66	**0.78**	**0.71**	**0.82**	0.69	0.48*	**0.76**	0.64	1									
	K	0.67	**0.84**	0.53	**0.82**	**0.7**	0.59	0.52	0.53	0.69	1								
	Mn	0.67	0.66	0.43*	0.51	**0.94**	0.61	0.65	**0.85**	**0.73**	**0.7**	1							
	Fe	0.53	0.58	0.36**	0.51	**0.86**	0.6	0.62	**0.8**	**0.71**	0.56	**0.97**	1						
	Cu	0.72	**0.78**	**0.78**	0.62	**0.87**	0.54	**0.97**	**0.81**	**0.78**	**0.7**	**0.88**	**0.84**	1					
W_in	DTT	0.44*	0.48	-0.23**	0.55	0.57	0.26**	0.38**	0.5	**0.87**	0.50*	0.66	0.63	0.56	1				
	K	0.6	0.6	0.42*	0.61	**0.76**	0.54	0.30**	0.65	0.66	**0.94**	**0.74**	0.69	0.61	0.50*	1			
	Mn	0.43*	0.66	0.31**	0.37**	**0.79**	0.64	0.43*	**0.74**	0.62	0.62	**0.96**	**0.95**	**0.75**	0.59	**0.7**	1		
	Fe	0.49*	0.57	0.35*	0.49*	**0.86**	0.57	0.59	**0.8**	**0.7**	0.55	**0.96**	**0.9995**	**0.84**	0.64	0.69	**0.95**	1	
	Cu	**0.72**	**0.78**	**0.78**	0.61	**0.88**	0.54	**0.97**	**0.82**	**0.78**	**0.7**	**0.89**	**0.85**	**0.9999**	0.56	0.63	**0.76**	**0.84**	1

Historical Data

The final section of Appendix B includes local historical measurement data to compare to the concentration measurements collected during the study. Figure B.6 and B.7 shows the concentration data from the Georgia state run South Dekalb site for CO and NO_2 respectively. Figure B.8 and B.9 shows the concentration data from the SEARCH JST site for CO and NO_2 respectively. Figure B.10 shows the annual average concentrations for CO and NO_2 at the JST and EPD South Dekalb sites.

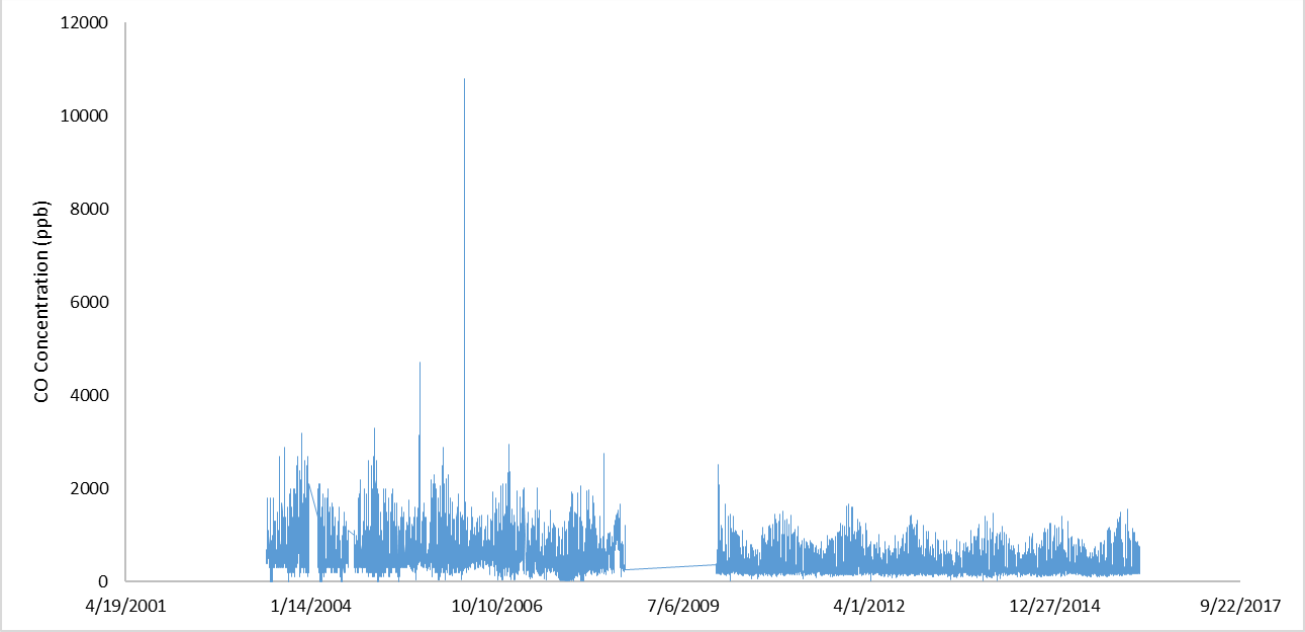

Figure B.6. Time series of hourly CO concentrations from the EPD South Dekalb (SDK) site from 2003 to 2015.

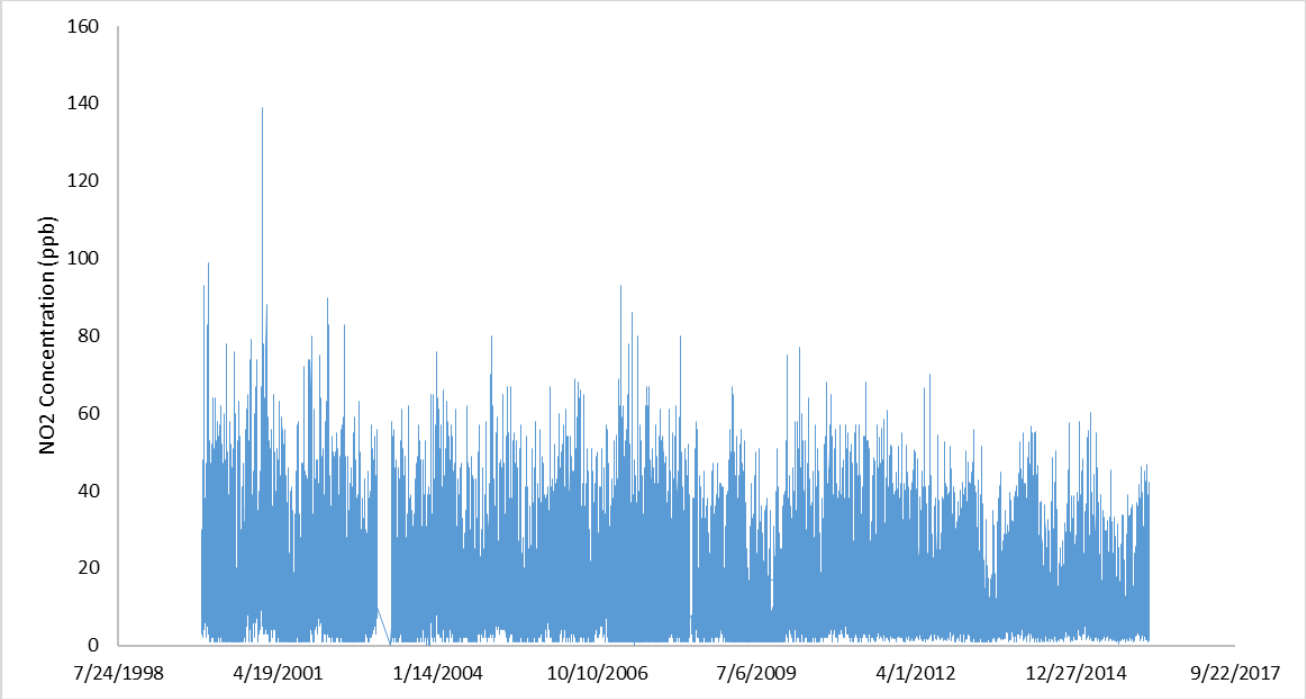

Figure B.7. Time series of hourly NO_2 concentrations from the EPD South Dekalb (SDK) site from 1999 to 2015.

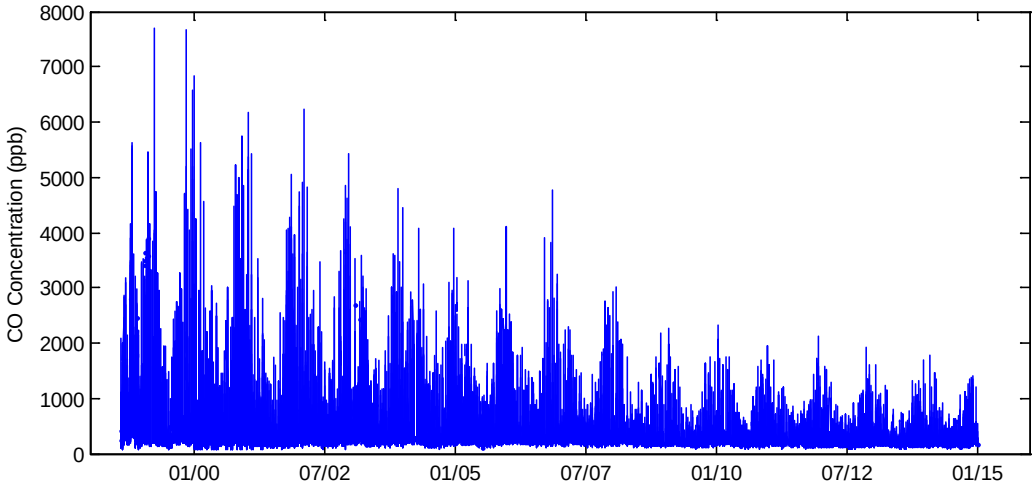

Figure B.8. Time series of hourly CO concentrations from the JST site from 1998 to 2014.

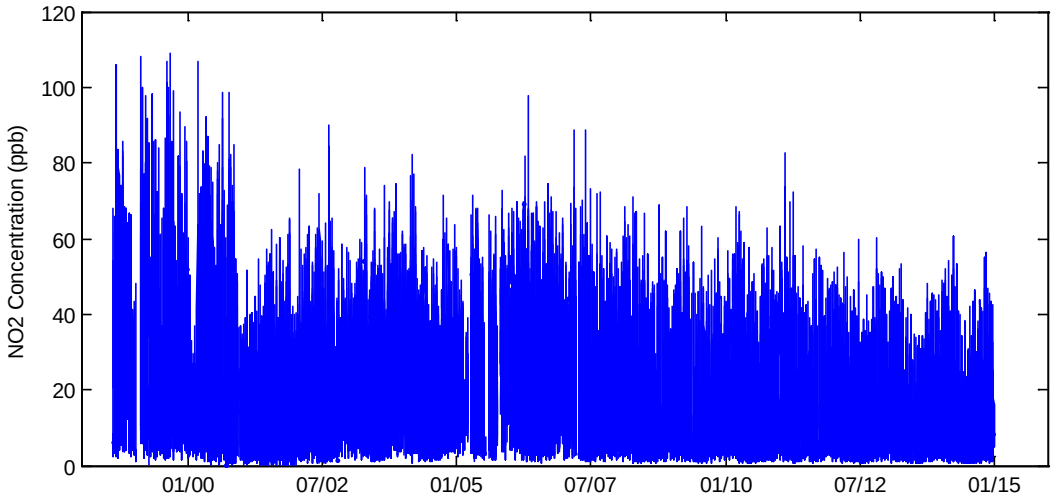

Figure B.9. Time series of hourly NO_2 concentrations from the JST site from 1998 to 2014.

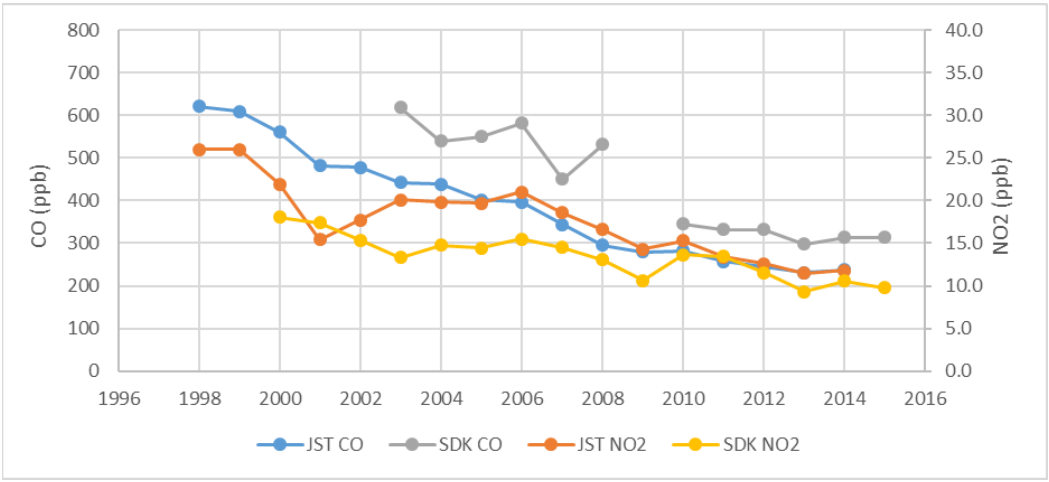

Figure B.10. Annual average concentrations for CO and NO_2 at the JST and EPD SDK sites.

Reference for Appendix B: U.S. DOT, U.S. Department of Transportation, *https://www.transportation.gov/*.

Appendix C: Low-Cost Sensors

The particulate matter sensors we used were from Shinyei Technology (Kobe, Japan); the three models used were PPD42NS (LOD: 1 µm), PPD20V (LOD: 1 µm), and PPD60PV (LOD: 0.5 µm). The sensors measure particle concentration by light scattering using an infrared LED light source and a photodiode array with lens to measure the scattered light at around 45 degrees. Although a limit of detection (LOD) was specified for each sensor, the manufacturer did not provide an equation to convert recorded electrical signals to particle concentrations, and little information was provided on how these LODs were developed (Shinyei Kaisha 2002; Shinyei Technology Co. 2010; Shinyei Technology Co. 2013). Therefore, a calibration needed to be developed before the sensors could be deployed based on the concentrations recorded by a reference instrument. The sensors were all calibrated to a TEOM (Thermo Scientific, USA) to convert the electrical signals into PM concentrations. The TEOM was operated with $PM_{2.5}$ inlet cyclones. The sensors are not size selective; however, they are compared with a $PM_{2.5}$ reference instrument in order to assess their performance as a surrogate measurement for $PM_{2.5}$ for future use.

The gas sensors are electrochemical cells that generate a current that is supposed to be linearly proportional to the concentration of the pollutant. In order to determine the change in current over time, the currents of two electrodes are recorded and used in the manufacturer-provided calibration curve specific to each individual sensor. When the electrodes are exposed to air, they undergo a specific redox reaction to generate a voltage. A third electrode is enclosed in the sensor to provide a reference for the current without exposure to air.

The format of the calibration curves for CO, NO, and NO_2 supplied by the manufacturer are shown by Equation C.1, and the values for each gas are shown in Table C.1. The calibration of O_3 depends on the concentration of NO_2, and therefore the curve (Equation C.2) for O_3 includes an additional term.

Thus, for CO, NO, or NO_2:

$$[\text{Concentration of CO, NO, or } NO_2]\ (\text{ppb}) = ((\text{work} - a) - (\text{aux} - b))/d \qquad \text{(Eq. C.1)}$$

work: Voltage generated by the gas electrode (mV)

aux: Voltage generated by the reference electrode (not exposed to air) (mV)

a: Baseline reading from gas electrode (mV)

b: Baseline reading from the reference electrode (mV)

d: Sensor's sensitivity to the gas being measured (mV/ppb)

Table C.1. Calibration Values for Gas-Pollutant (CO, NO, NO_2) Sensors Used

	a	*b*	*d*
CO	280	279	0.243
NO	271	270	0.352
NO_2	298	294	0.456

Similarly, for O_3:

$$O_3 = ((\text{work} - a) - (\text{aux} - b) - [NO_2]^*c)/d \quad \text{(Eq. C.2)}$$

work: Voltage generated by the O_3 electrode (mV)

aux: Voltage generated by the reference electrode (not exposed to ozone) (mV)

$[NO_2]$: The concentration of NO_2 (ppb)

a: Baseline reading from O_3 electrode (mV)

b: Baseline reading from the reference electrode (mV)

c: Sensor's sensitivity to NO_2 (mV/ppb)

d: Sensor's sensitivity to O_3 (mV/ppb)

Table C.2. Calibration Values for the O_3 Pollutant Sensor Used

	a	*b*	*c*	*d*
O_3	412	407	0.333	0.222

In addition to the pollution sensors, Sensirion AG temperature and SHT15 RH sensors (Staefa, Zurich, Switzerland) were used to measure the conditions in each sampling box. The temperature was measured by band-gap displacement, and RH was measured using a capacitive sensor (Sensiron 2010).

Rotation Schedule

Table C.3 shows the rotation schedule for the four boxes along with the number of observations collected during each rotation. This allowed the sensors to be assessed at various distances away from the highway source.

Table C.3. Multisensory Units Rotation Schedule

Box Number	1	2	3	4
Sensors	PM PPD20V	NO NO_2 CO O_3 PM PPD20V	PM PPD20V PM PPD42NS PM PPD60PV	PM PPD20V
NDI			Rotation 1 11/4-11/25	Rotation 2 11/25-12/9
NDO	Rotation 3 12/9-12/17	Rotation 1 11/15-11/25		Rotation 3 12/9-12/17
FDO	Rotation 1 11/20-11/25	Rotation 3 12/9-12/17	Rotation 2 11/25-12/9	
RDS		Rotation 2 11/25-12/9	Rotation 3 12/9-12/17	Rotation 1 11/20-11/25

CO, NO, and NO_2 Sensors

Unit 2 contained the gas phase sensors and was rotated to three sites: NDO, RDS, and FDO. The linear correlation with the reference instrument is included in Table C.4 along with the average difference between the reference instrument and the sensor, and the 95% confidence interval of the difference.

Table C.4. Linear Correlations between Gas Sensors and Reference Instruments

		NDO			RDS			FDO		
Species		CO	NO	NO_2	CO	NO	NO_2	CO	NO	NO_2
Linear Regression (Sensor (ppb) = a*Ref(ppb) + b)	Slope (a)	0.76	0.69	2.11	0.75	0.81	3.09	0.62	0.87	3.89
	Intercept (b)	-62.33	-3.25	-28.91	-37.71	-6.20	-19.09	75.36	-5.55	-55.87
R^2		0.85	0.86	0.78	0.90	0.92	0.54	0.51	0.79	0.78
N (Hourly Average)		268	272	272	1666	334	334	227	189	189
Average Difference [Mean(ref-sensor)]		148.11	6.89	-1.93	160.28	11.13	-33.31	-15.09	7.07	-8.00
95% confidence interval of the difference [1.96*std dev(ref-sensor)]		174.04	12.34	41.11	291.40	19.64	107.10	86.75	9.90	38.13

Particulate Sensors

Unit 2 contained a single PM sensor at the NDO site, and unit 3 contained the three different models of the PM sensors used during the study. The linear regressions between the reference instrument and the sensors helped compare the various models for accuracy (Table C.5).

Table C.5. Linear Correlations between PM Sensors and Reference Instruments

		NDO	NDI		
Model		PPD20V	PPD42NS	PPD20V	PPD60PV
Linear Regression (Sensor (ppb) = a*Ref(ppb) + b)	Slope (a)	0.79	0.53	0.91	0.80
	Intercept (b)	3.72	2.66	1.16	1.69
R^2		0.41	0.60	0.83	0.77
N (Hourly Average)		123	122	122	110
Average Difference [Mean(ref-sensor)]		-1.74	0.59	0.55	0.22
95% confidence interval of the difference [1.96*std dev(ref-sensor)]		10.65	3.81	2.49	2.77

O_3 Sensor

The O_3 sensor was also sent with a manufacture-calibration determined for the specific sensor. Figure C.1 shows the concentration after applying the calibration. The majority of the concentration values were negative, and the sensor did not capture the peaks observed by the reference instrument.

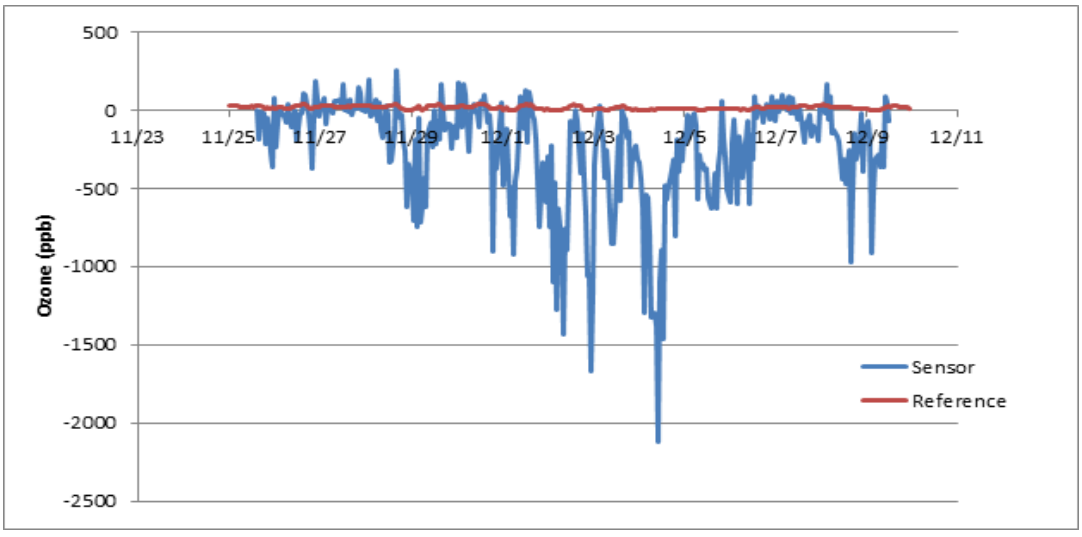

Figure C.1. Time series of O_3 sensor and relevant O_3 reference instrument at the RDS site.

The O_3 calibration curve relies on the NO_2 concentration (Eq. C.2) from the NO_2 sensor. Because the sensor was overestimating the NO_2 concentration, the O_3 concentration was calculated again using the reference analyzer NO_2 concentration values to show how dependent the O_3 concentration is on the accuracy of the NO_2 sensor or its calibration. Figure C.2 shows that the recorded concentration does depend on the NO_2 concentration, and by using a more accurate NO_2 concentration, the O_3 sensor now shows the peaks seen by the reference instrument. There are, however, still a significant number of negative values.

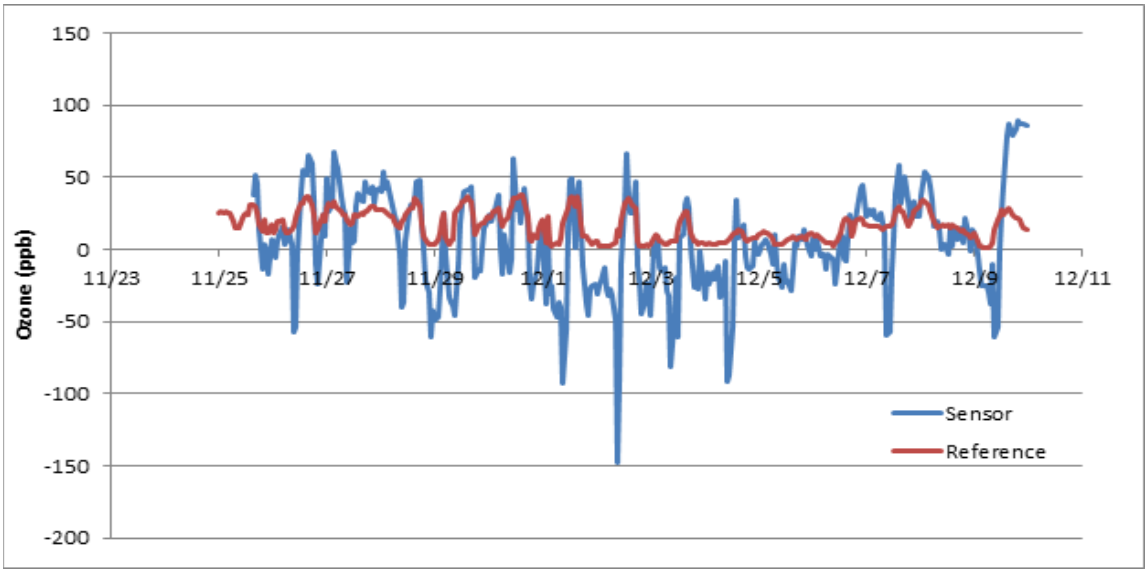

Figure C.2. Time series of O_3 sensor concentration using the reference instrument NO_2 concentration and relevant O_3 reference instrument at the RDS site.

Alternatively, the O_3 sensor data was corrected using a multi-variable regression. First the O_3 sensor concentration data was calculated using the manufacturer calibration curve and the NO_2 sensor concentration measured. The raw O_3 concentration data were calibrated using the exponential function found between the sensor concentration and the reference instrument. The initial calibration used is in the first row of Table C.6. The correlation improves when the new O_3 data set is compared with that of the reference instrument. The second step was to use a multi-variable calibration found using the new data set, temperature, and RH data. The final correlation is the linear regression between the O_3 data corrected with both calibration steps and the reference instrument.

Table C.6. Progression of Correlations as O_3 Sensor Results are Calibrated

	Regression (N = 334)	R^2
Initial Correlation	RawSensor (ppb) = 266.48*ln(Ref(ppb)) – 915.01	0.40
Exponential Calibration Step	Sensor1 (ppb) = EXP((RawSensor + 915.01) / 266.48)	--
Correlation after Exponential Calibration	Sensor1 (ppb) = 0.93*Ref(ppb) + 4.80	0.43
Multi-variable Calibration Step	Sensor2 (ppb) =Sensor (ppb) * 0.38 + T * 0.16 + RH * –0.24 + 21.83	--
Correlation after Multi-variable Calibration	Sensor2 (ppb) = 1*Ref(ppb)	0.68

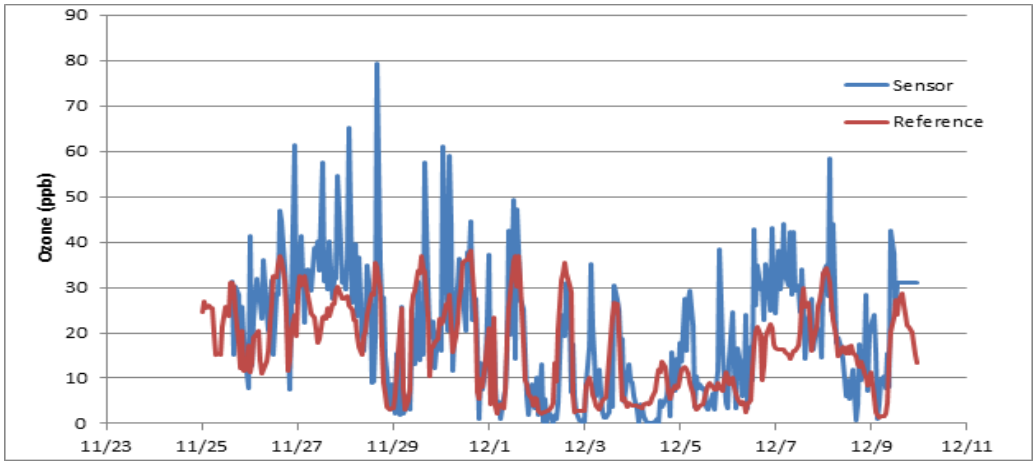

Figure C.3. Time series of O_3 sensor concentration after applying the exponential calibration and relevant O_3 reference instrument at the RDS site.

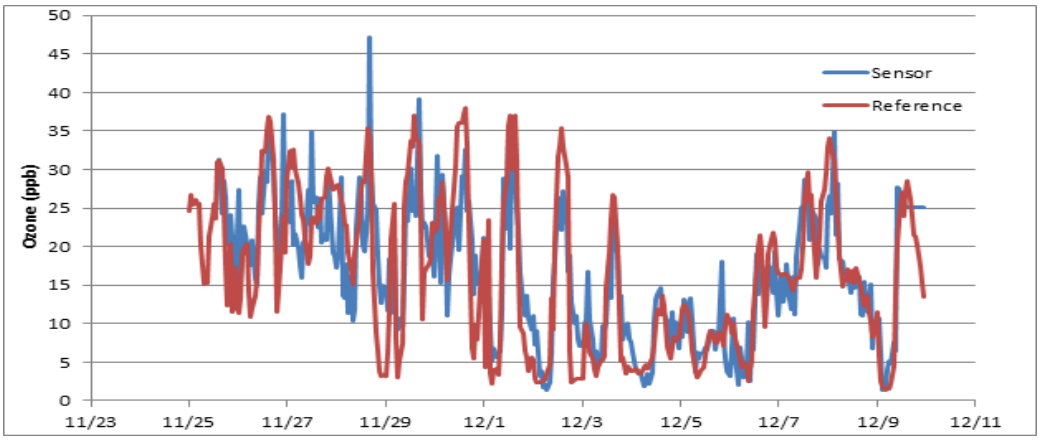

Figure C.4. Time series of O_3 sensor concentration after applying the multi-variable calibration that used the exponentially calibrated sensor data, temperature, RH, and relevant O_3 reference instrument at the RDS site.

References for Appendix C

Shinyei K. 2002. Product specifications PPD20V. In: SP-30-E-99007, 1-6. http://www.gvzcomp.it/index.php/en/fis?format=raw&task=download&fid=459.

Shinyei Technology Co. L. 2010. Specification sheet of PPD42NS. http://www.shinyei.co.jp/stc/eng/optical/main_ppd42.html

Shinyei Technology Co. L. 2013. Product specifications PPD60PV-T2. In: SP-30-E-08003(V01). http://www.shinyei.co.jp/stc/eng/optical/main_ppd60pv.html

Appendix D: RLINE Calibration

The DRIVE study focused on exposure to primary traffic emissions, and although measurements were collected in a traffic emissions hotspot, personal exposure monitoring necessarily measured overall pollutant exposure as opposed to exposure to traffic emissions specifically. In order to quantify traffic-related exposures, GPS location tracking from the personal monitoring and on-road dispersion modeling was used. The U.S. EPA–developed fine-scale dispersion model RLINE (Research LINE source model [Batterman et al. 2014b; Snyder et al. 2013]) was used to provide the hourly mobile source impacts on the CO, NO_x, and $PM_{2.5}$ concentrations across the whole study domain at a 25-m x 25-m grid resolution. An alternative dispersion model, AERMOD (AMS/EPA Regulatory Model, [EPA 2004]), was initially considered for use in generating exposure estimates; however, AERMOD handles line source emissions by characterizing the emissions as being from a series of rectangles, while RLINE was developed specifically for line sources, such as roadways, and has been evaluated using data from roadways, so we used RLINE instead. It is important to note that there are limitations to the use of RLINE and other dispersion models in this or other applications. The model simulates the concentration fields of primary pollutants as they are affected by on-road emission. Although RLINE simulates the transport of primary $PM_{2.5}$ mobile emissions and the resulting concentration fields, the lack of chemistry in the model means it does not include secondary $PM_{2.5}$ formation and O_3 chemistry. Secondary $PM_{2.5}$ formation occurs photochemically as mobile VOC and NO_x emissions react to form lower-vapor-pressure products (Gordon et al. 2013; May et al. 2013a,2013b, 2014; Ranjan et al. 2012; Stelson and Seinfeld 1982; Tkacik et al. 2014; Zhao et al. 2015, 2016), and O_3 chemistry affects the concentration of NO_x as well as the fraction of NO_x that is converted from NO to NO_2. In addition, deposition is not included as a factor that effects concentration, though over the short time scales involved here, this process is likely of lesser importance.

The RLINE model domain included on-road mobile source emissions from the entire Atlanta region, with a fine-resolution 6.5 km by 2.5 km grid centered on the GIT campus. Emissions from roads outside of the fine grid domain are included in the modeling, though the concentration maps provided presented in this document focus on the fine grid area. Emission inputs used were the 2010 average link-based, on-road mobile source emissions in the 20-county region surrounding metro Atlanta developed by the Atlanta Regional Commission (ARC) using its traffic demand and mobile source emissions modeling (D'Onofrio 2015; Zhai et al. 2016). Figure D.1 shows a map of the simulated area and the 20-county region. ARC estimated the emissions, in g/m/s, of CO, NO, and $PM_{2.5}$ for 43,712 links based on modeled traffic volume, vehicle speed, and fleet demographics. The U.S. EPA's Motor Vehicle Emission Simulator (MOVES) modeling system (Ayala et al. 2012; Batterman et al. 2014a; U.S. EPA 2014) was then used to estimate annual emissions from each link.

The hourly meteorological input data were developed using AERMET (Cimorelli et al. 2005; U.S. EPA 2004). The surface meteorological data measurements were from the National Weather Service at the Hartsfield-Jackson Atlanta International Airport and preprocessed using AERMINUTE (U.S. EPA 2015). The upper air data measurements were from the Peachtree City Falcon Field Airport. Because steady-state dispersion models tend to overestimate concentrations during calm air conditions, the EPA suggests resetting any wind speed less than 1 m/s to 1 m/s (U.S. EPA 2000). Between September 1, 2014, and December 31, 2014, there were 88 hours with a wind speed below 1 m/s. The raw RLINE spatial plots are provided when the wind fields were not adjusted to have all wind velocities above 1 m/s (Figures D.2 –D.4), and the effects of the wind speed adjustment are shown (Figures D.5–D.7).

Additional corrections were necessary because the ARC modeling was for 2010. Therefore, the 2010 link emissions were scaled to 2014 using the mobile emissions ratio of 2014 to 2010 from MOVES 2014 (Table D.1) (U.S. EPA 2014). The average diurnal emissions profile was used to provide hourly link-based emissions (Figure D.8 and Table D.2). Accounting for the diurnal variation in emissions is important because in the evening when the boundary layer is low, if the annual average traffic volume is used, the estimated pollutant concentrations are biased high (Zhai et

al. 2016). Using the yearly and diurnal adjustments leads to the spatial fields shown in Figures D.9–D.11.

Previous research has shown that locally elevated simulated concentration levels co-occur with specific meteorological scenarios (Perry et al. 2005; Venkatram et al. 2004, 2013a, 2013b). In addition, unrealistically high concentrations were observed on and very near the main highway emissions source. In order to correct for unreasonably high concentrations in the RLINE output, ground-level measurements were used to scale the results. This process led to concentration levels that more accurately represented pollutant concentrations due to the direct impact of traffic emissions across the study domain. The simulated values were compared with observations to develop linear calibrations to adjust the RLINE results (Figure D.12, Table D.3). The final fields with the applied linear regression and removed local background are shown in Figures D.13 and D.14. Table D.4 provides a summary of the correlation between the hourly RLINE results and the observations. The low correlations are likely driven by the very large diurnal variation simulated by RLINE (Figure D.15).

Dispersion modeling results from RLINE provided a complete spatial distribution of CO, NO_x, $PM_{2.5}$, and $OP^{WS\text{-}DTT}$ for each hour during the period September 1, 2014, to December 31, 2014. RLINE filled a critical role in providing spatiotemporal fields of how mobile sources affect the concentrations of these pollutants that are not directly available from the ambient or personal monitoring conducted as part of DRIVE or from associated monitoring. By matching the GPS location and time to the RLINE results, the estimated hour-by-hour ambient exposures could be mapped for each student participant in the study. Further, these data provided an additional approach to assessing the impact of meteorology and traffic-related factors on air quality in the study domain.

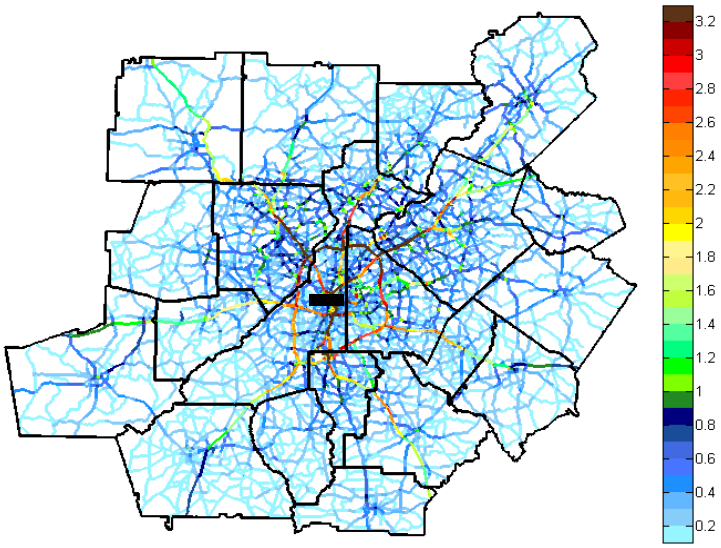

Figure D.1. $PM_{2.5}$ emissions by mobile sources for 20-county area around Atlanta (g/m/s).

Raw RLINE Results

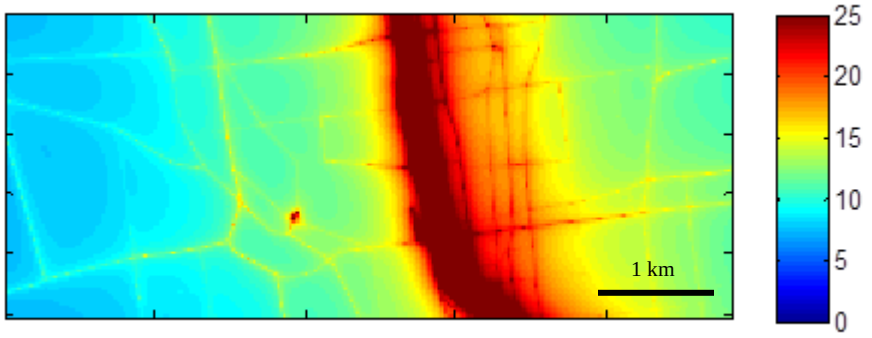

Figure D.2. Uncalibrated $PM_{2.5}$ RLINE results (µg /m^3).

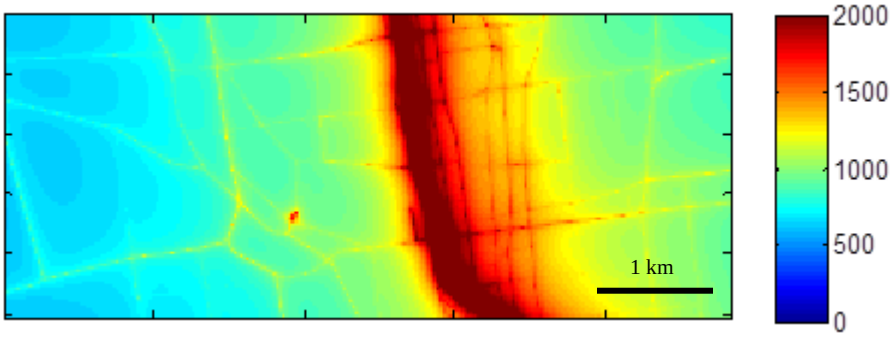

Figure D.3. Uncalibrated CO RLINE results (ppb).

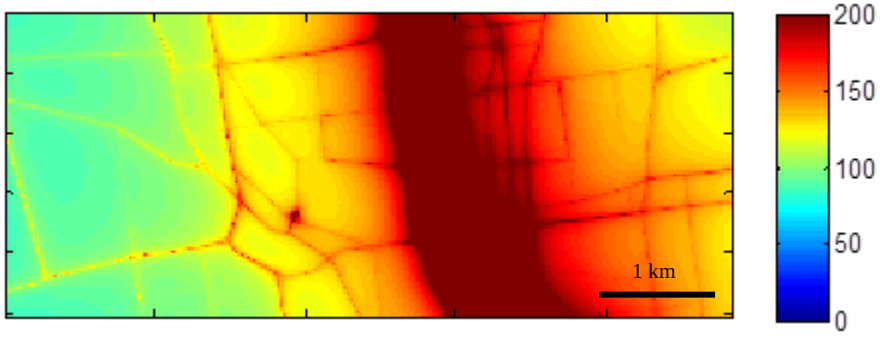

Figure D.4. Uncalibrated NO_x RLINE results (ppb).

In order to avoid unrealistically high concentration estimates at low wind speeds, the U.S. EPA recommends "that wind speeds less than 1 m/s be reset to 1 m/s for use in steady-state dispersion models" (U.S. EPA 2000).

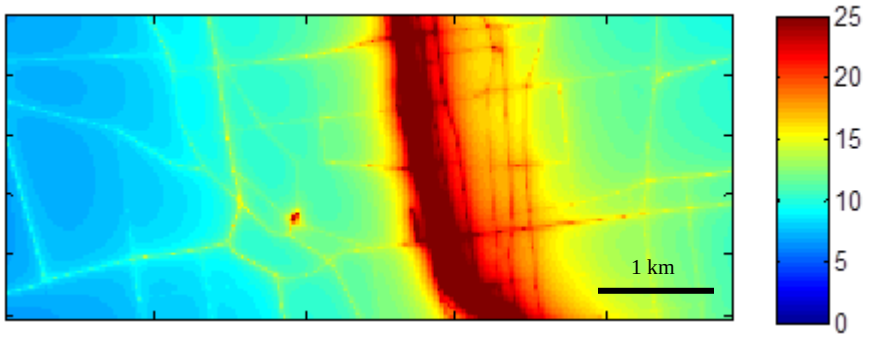

Figure D.5. $PM_{2.5}$ RLINE with all wind speeds 1 m/s or above (µg /m^3).

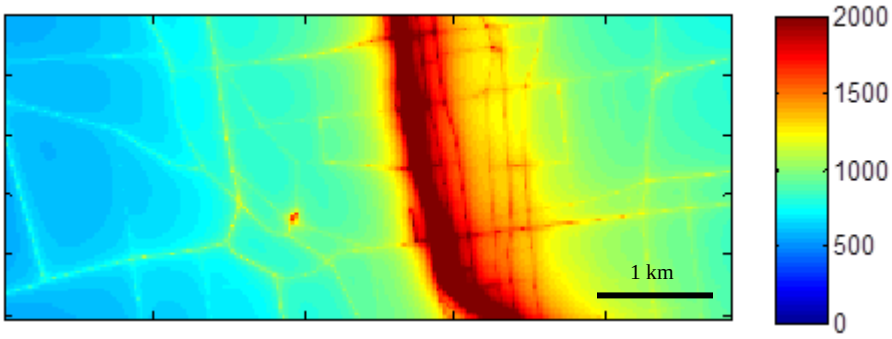

Figure D.6. CO RLINE with all wind speeds 1 m/s or above (ppb).

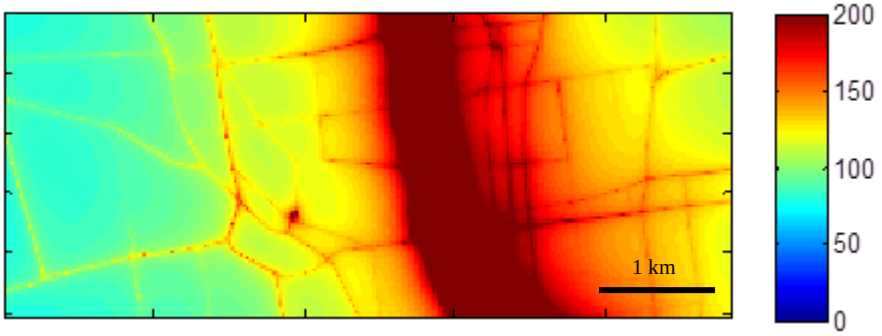

Figure D.7. NO_x RLINE with all wind speeds 1 m/s or above (ppb).

The most recent source emissions file was from 2010 and includes all road emissions in the 20-county region surrounding the metro Atlanta area. In order to account for reduced emissions since 2010, a 2014-to-2010 mobile emissions ratio was applied, based on results from MOVES (U.S. EPA 2014). Further, to develop hourly RLINE results, a 24-hour-emissions adjustment was applied, based on the annual average diurnal profile.

Table D.1. Ratio of 2014 Annual Average to 2010 Annual Average from MOVES2014

$PM_{2.5}$	NO_x	CO
0.65	0.69	0.81

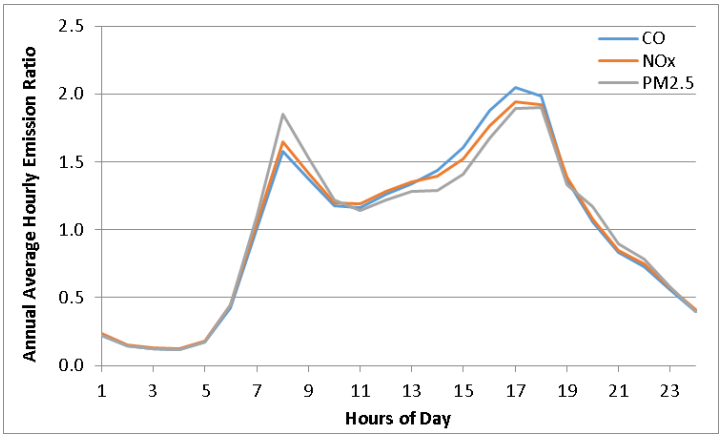

Figure D.8. Ratio of 2010 average diurnal profile to average 24-hour mean.

Table D.2. Ratio of 2010 Hourly Emissions to 24-Hour Mean

Hour	CO Ratio	NO_x Ratio	$PM_{2.5}$ Ratio
1	0.22	0.23	0.22
2	0.15	0.15	0.15
3	0.12	0.13	0.12
4	0.12	0.12	0.12
5	0.17	0.18	0.17
6	0.42	0.44	0.45
7	1.01	1.06	1.11
8	1.58	1.65	1.85
9	1.38	1.42	1.53
10	1.17	1.20	1.22
11	1.16	1.19	1.14
12	1.26	1.28	1.22
13	1.34	1.35	1.28
14	1.44	1.39	1.29
15	1.61	1.52	1.41
16	1.88	1.76	1.67
17	2.05	1.94	1.89
18	1.98	1.92	1.90
19	1.37	1.39	1.33
20	1.06	1.08	1.17
21	0.83	0.85	0.89
22	0.73	0.75	0.78
23	0.56	0.58	0.58
24	0.39	0.41	0.40

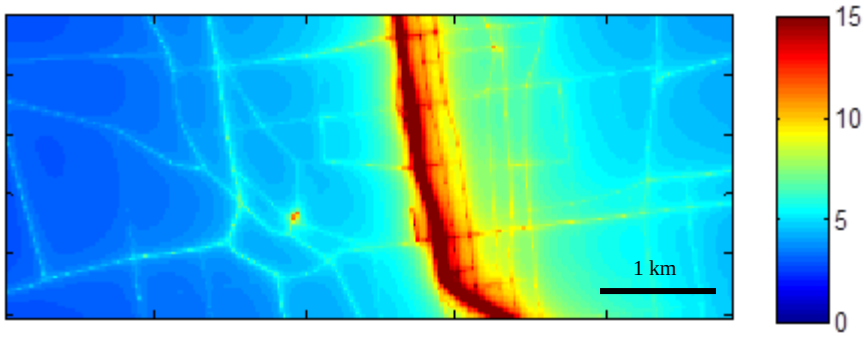

Figure D.9. $PM_{2.5}$ RLINE with yearly and diurnal emission adjustments (µg/m^3).

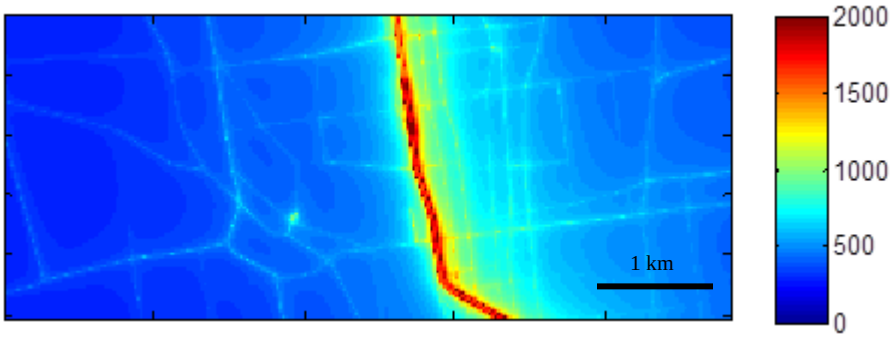

Figure D.10. CO RLINE with yearly and diurnal emission adjustments (ppb).

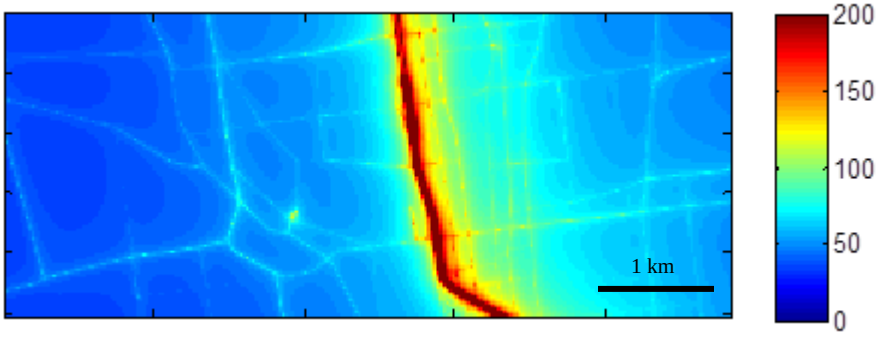

Figure D.11. NO_x RLINE with yearly and diurnal emission adjustments (ppb).

After calibration, the CO, NO_x, $PM_{2.5}$, and $OP^{WS\text{-}DTT}$ concentrations during September 1st to December 31st still showed very rapid decreases with decreasing proximity to the high source region (the Connector), as observed from the monitoring results in the DRIVE study. Again, the modeled spatial distribution of each pollutant included the impact of meteorology and timing and distributions of mobile source emissions on concentrations, but did not include other sources, or vehicle emissions outside the 20-county region (the 20-county area dominates on-road mobile emissions in the region), and pollutant chemistry or deposition.

To further correct the data, a linear regression was applied using the observations from the sampling sites.

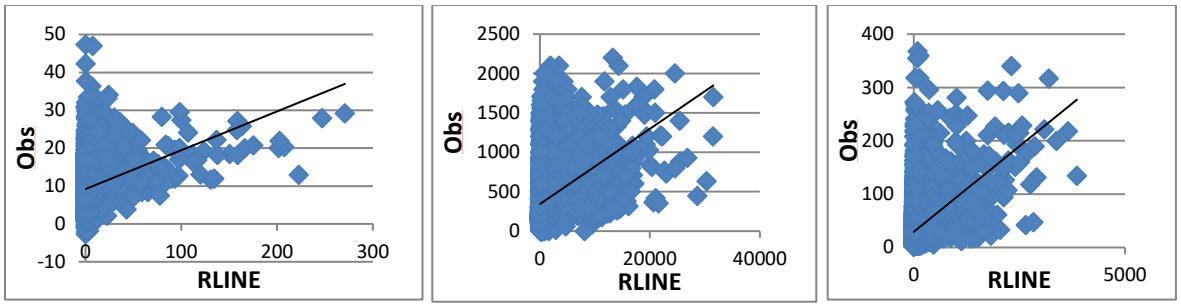

Figure D.12. Regression to correct $PM_{2.5}$, CO, and NO_x RLINE data with observations.

Table D.3. Linear Calibration

Species		$PM_{2.5}$ (µg /m^3)	CO (ppb)	NO_x (ppb)
Linear Regression	Slope (a)	0.1025	0.0478	0.0642
(Sensor (ppb) = a*Ref(ppb) + b)	Intercept (b)	9.19	343.02	29.37
R^2		0.0838	0.1148	0.1812
N (Hourly Average)		5027	14031	15019

The fields for all the directly simulated pollutant concentrations and derived measures were, not surprisingly, similar, showing high levels over and very near the freeway (Figure D.13). We also used the simulated results to develop the spatial IMSI field and $OP^{WS\text{-}DTT}$. The $OP^{WS\text{-}DTT}$ field was developed directly from the $PM_{2.5}$ field and the $OP^{WS\text{-}DTT}$/µg derived by Bates and colleagues (2015). Levels on the GIT campus were generally estimated to be low. Higher concentrations were found on the other side of the freeway, where more trafficked surface streets are found. However, the generally easterly winds still led to emissions from the Connector, affecting the campus. The highest levels were predicted when winds were low, such that the averages were dominated by concentrations occurring when winds and dispersion were both low (e.g., at night), even if the emissions were low. The presence of major surface streets surrounding the campus is seen, though at much lower levels than near the freeway (including at the near dorm). Simulated levels at the RFT site, far dorm, and JST site were relatively low. The average simulated impact of on-road mobile sources on $PM_{2.5}$ levels over the fine-scale domain was 0.57 µg/m^3; the hourly maximum was 79, occurring directly on the highway. For CO the same metrics were 24 ppb (average) and 3500 ppb (max.), and for NO_x they were 4.0 ppb and 560 ppb (Figure D.14).

a.

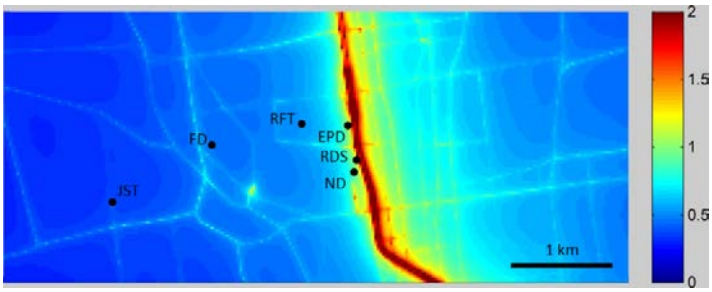
RFT
FD
EPD
RDS
ND
JST
1 km
2
1.5
1
0.5
0

b.

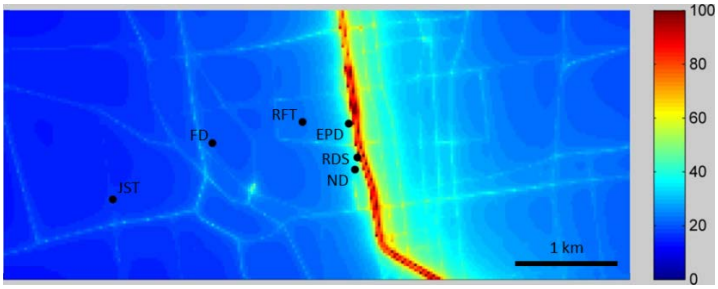
RFT
FD
EPD
RDS
ND
JST
1 km
100
80
60
40
20
0

c.

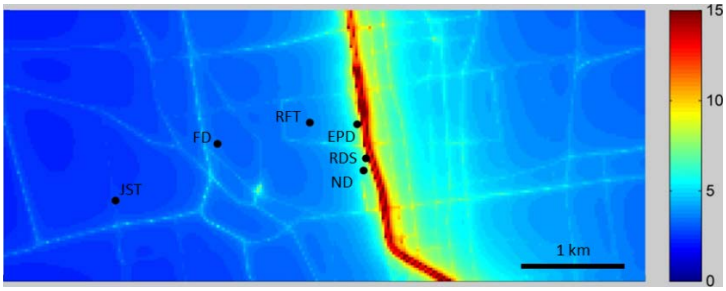
RFT
FD
EPD
RDS
ND
JST
1 km
15
10
5
0

d.

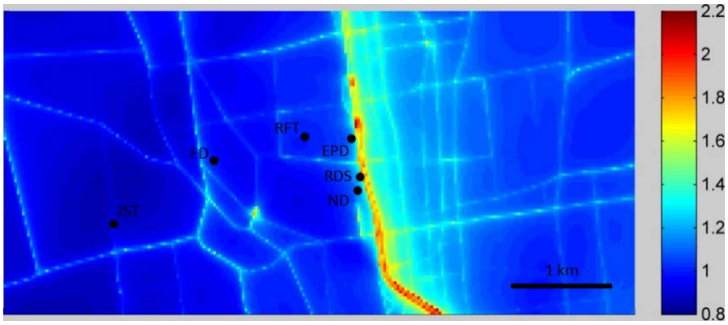
RFT
FD
EPD
RDS
ND
JST
1 km
2.2
2
1.8
1.6
1.4
1.2
1
0.8

e.

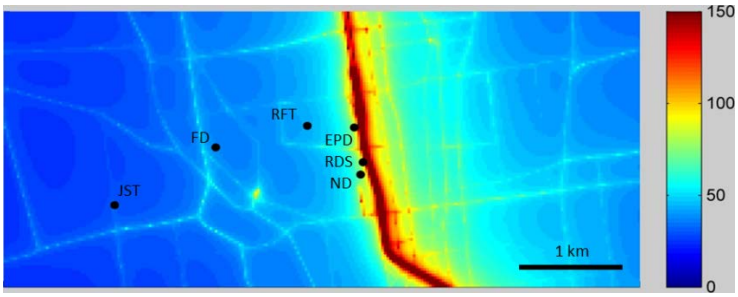

Figure D.13. Simulated study average pollutant concentration impacts from on-road mobile source emissions simulated by RLINE after calibration: (a) $PM_{2.5}$ (µg/m^3), (b) CO (ppb), (c) NO_x (ppb), (d) the IMSI, and (e) water-soluble OP from mobile emissions (pmol min^{-1} m^{-3}).

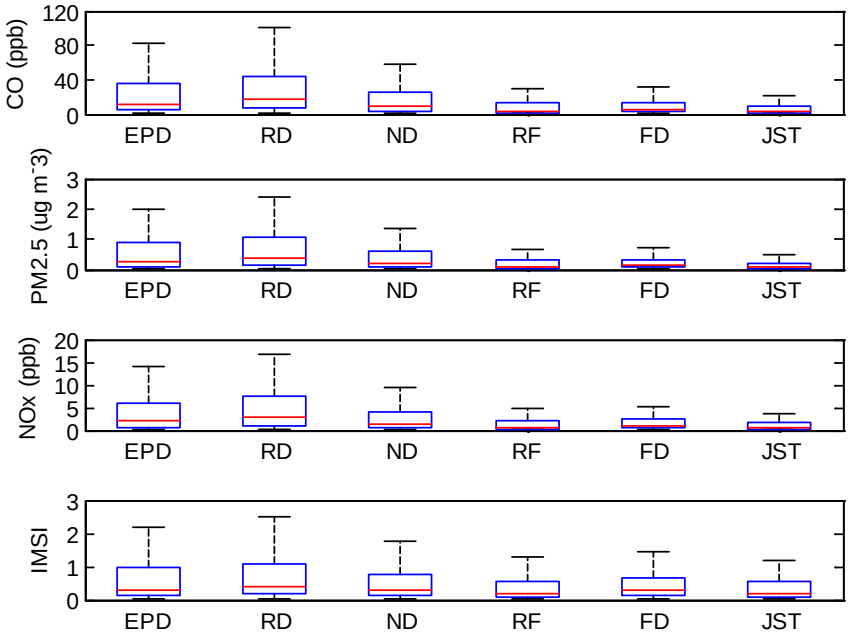

Figure D.14. Hourly mean RLINE concentration data, excluding all outliers outside the interquartile range for CO, $PM_{2.5}$, NO_x, and the IMSI developed from RLINE results from September 1, 2014, to December 31, 2014, at the sampling locations ordered by increasing distance from the highway source: (EPD) Georgia Department of Natural Resources Near-road Network Monitor [5 m], (RDS) Near-roadway stationary site [10 m], (NDO) Near Dorm outside [20 m], (NDI) near dorm inside [20 m], (RFT) rooftop lab [500 m], (FDO) far dorm outside [1.4 km], (FDI) far dorm inside [1.4 km], and (JST) urban background [2 km].

Although the RLINE results were calibrated using hourly measurements, the correlation with the observations remained low (R^2 = 0.07–0.20) for all three species (Table D.4). The diurnal profile highlights why the correlation between the simulated concentrations and measured concentrations was low (Figure D.15). The diurnal profiles for the calibrated RLINE results had strong concentration peaks at 7 A.M. and 6 P.M. and concentrations close to zero between 10 A.M. and 3 P.M. for all the species. Although the diurnal profiles for the measured pollutant concentrations also showed two clear peaks in the morning and evening, the drop in the middle of the day was not as dramatic and was not seen at the near-road sampling locations. Further investigation of means for

modifying parameterizations as well as calibrating RLINE is recommended. Future RLINE calibration might consider applying a separate calibration for each hour as opposed to a single calibration curve.

Table D.4. Linear Regression Correlation (R^2) between RLINE and Observations

	EPD	RDS	NDO	RFT	FDO	JST
CO	0.02	0.21	0.03	0.04	0.02	0.05
NO_x	0.03	0.06	0.04	0.03	0.03	0.07
$PM_{2.5}$	--	--	--	0.03	--	0.04

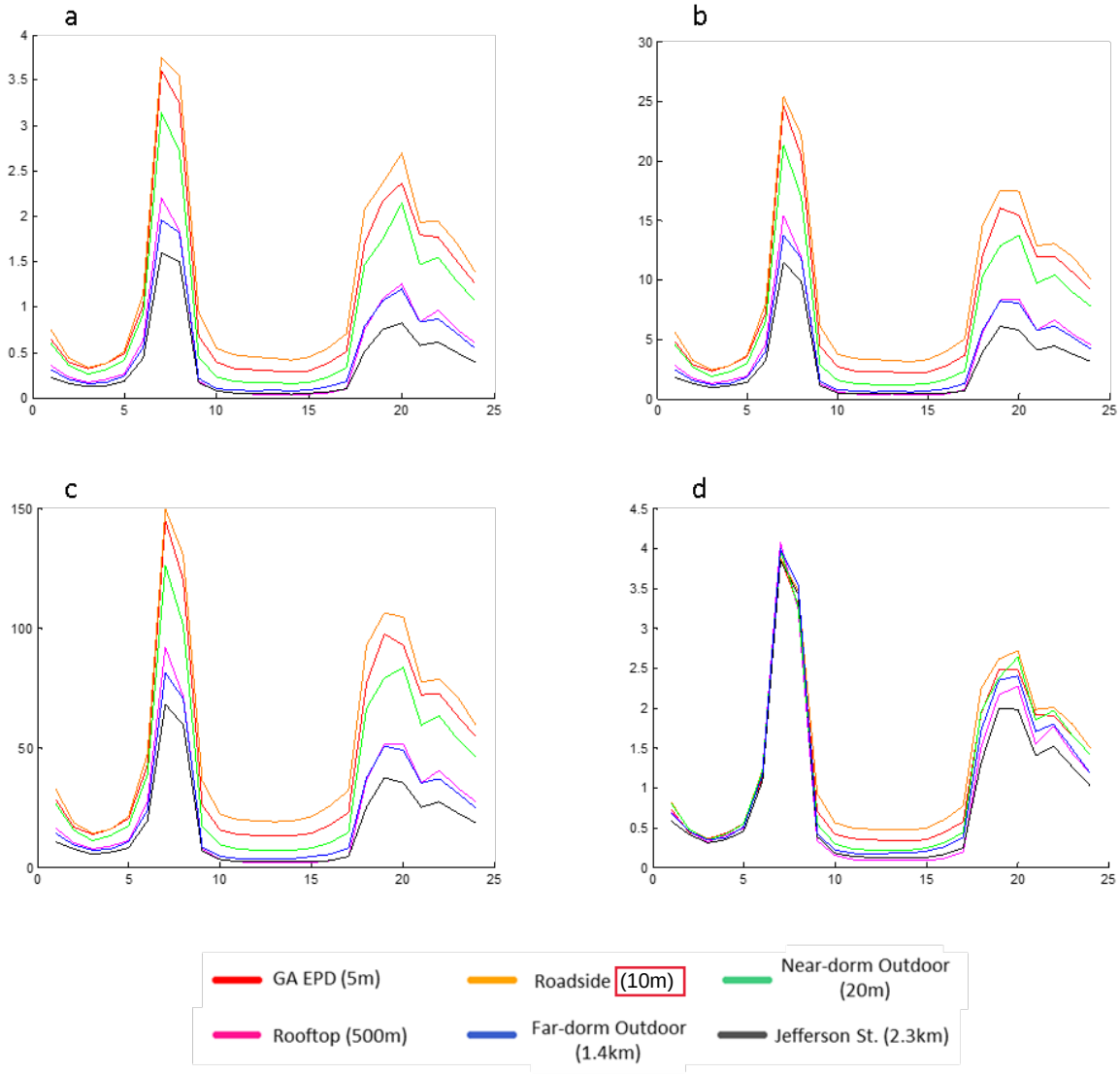

Figure D.15. Diurnal profile of RLINE results for (a) $PM_{2.5}$ (μg /m^3), (b) NO_x (ppb), (c) CO (ppb), and (d) the IMSI.

The DRIVE RLINE output clearly showed that the RLINE-simulated levels required calibration, due to model parameter errors, emissions inventory errors, or very likely both (Anderson et al. 2014; Fujita et al. 2012; Heist et al. 2013; Isakov et al 2004; Qian and Venkatram 2011; Snyder et al. 2013; Venkatram et al. 2013a; Venkatram and Schulte 2014). In particular, the very near-field levels were high compared with observations, sometimes very high; this was particularly true during periods of higher stability. In a prior study, over a larger domain, it was also found that the near-field levels were quite high, while areas well away from the city had simulated levels significantly lower than observations of traffic-related species, indicating that the model overestimates the near-field concentration gradients (Zhai et al. 2016). Thus, model output calibration was required to better capture the concentration fields on campus, though the correlation of hourly values between observations and simulated levels remained low. One advantage of such an exercise is it also provided an estimate of the urban background that would exist without mobile source emissions and if there are likely inventory biases in one species versus another. The intercepts suggest that the urban background CO and NO_x are similar to rural observations, supporting the notion that mobile sources dominate those species emissions in Atlanta, in line with the emissions inventories. The ratios of the slopes of the regressions suggest that the $PM_{2.5}$ emissions estimates are biased low when compared with the estimates of CO and NO_x. This does not mean they are biased high compared with actual emissions, as NO_x and CO emissions may be lower than estimated. Using this type of analysis to help assess emissions inventories may be of interest but would require further investigation and would benefit from longer-term and more additional observations than were used here. Further, our results emphasize the need to further refine the parameterizations in RLINE, particularly during periods of low dispersion. The RLINE-simulated concentrations captured, but overemphasized, the diurnal trends in the traffic-related pollutants modeled.

Using linear calibration provides other useful information in addition to providing spatiotemporal fields of mobile source emissions impacts. The slope is indicative of a combination of the degree of misspecification of the diffusion and potential biases in the emissions. The regression slopes were 0.10, 0.05, and 0.06 for $PM_{2.5}$, CO, and NO_x, respectively, suggesting that the emissions estimates were biased high or the dispersion parameters biased low. The intercept is indicative of what urban concentration levels would be without mobile source emissions. In this case, the CO intercept was 343 ppb, which is in line with the findings of Zhai and colleagues (2016), and similar to background levels (Seinfeld and Pandis 2006). NO_x was 29 ppb, in line with other measurements in the area, and $PM_{2.5}$ was 9 μg/m^3, which was in line with other analyses and similar to the measurements at the rural site outside Atlanta (Blanchard et al. 2013a, 2013b, 2014, 2016; Henneman et al. 2015; Hidy et al. 2014; Watson et al. 2015). Although it is difficult to say what is the most important factor of the slope or intercept when examining any one pollutant, comparing all three can suggest if any one of the emissions is biased in comparison with the others. Our results suggest that, compared with $PM_{2.5}$, CO, and NO_x emissions, the estimates may be biased high, though such results should not be taken as conclusive but suggestive of further study.

References for Appendix D

Anderson DC, Loughner CP, Diskin G, Weinheimer A, Canty TP, Salawitch RJ, et al. 2014. Measured and modeled CO and NOy in DISCOVER-AQ: An evaluation of emissions and chemistry over the eastern US. Atmos Environ 96:78–87.

Ayala A, Brauer M, Mauderly JL, Samet JM. 2012. Air pollutants and sources associated with health effects. Air Qual Atmos Health 5:151–167.

Bates JT, Weber RJ, Abrams J, Verma V, Fang T, Klein M, et al. 2015. Reactive oxygen species in atmospheric particulate matter suggest a link to cardiorespiratory effects. Environ Sci Technol 49(22): 13605-13612.

Batterman S, Chambliss S, Isakov V. 2014a. Spatial resolution requirements for traffic-related air pollutant exposure evaluations. Atmos Environ 94:518–528.

Batterman S, Ganguly R, Isakov V, Burke J, Arunachalam S, Snyder M, et al. 2014b. Dispersion modeling of traffic-related air pollutant exposures and health effects among children with asthma in Detroit, Michigan. Transport Res Rec 2452:105–113.

Blanchard CL, Hidy GM, Tanenbaum S, Edgerton ES, Hartsell BE. 2013a. The Southeastern Aerosol Research and Characterization (SEARCH) Study: Spatial variations and chemical climatology, 1999-2010. J Air Waste Manage Assoc 63:260–275.

Blanchard CL, Hidy GM, Tanenbaum S, Edgerton ES, Hartsell BE. 2013b. The Southeastern Aerosol Research and Characterization (SEARCH) Study: Temporal trends in gas and PM concentrations and composition, 1999-2010. J Air Waste Manage Assoc 63:247–259.

Blanchard CL, Chow JC, Edgerton ES, Watson JG, Hidy GM, Shaw S. 2014. Organic aerosols in the southeastern United States: Speciated particulate carbon measurements from the SEARCH network, 2006-2010. Atmos Environ 95:327–333.

Blanchard CL, Hidy GM, Shaw S, Baumann K, Edgerton ES. 2016. Effects of emission reductions on organic aerosol in the southeastern United States. Atmos Chem Phys 16:215–238.

Cimorelli AJ, Perry SG, Venkatram A, Weil JC, Paine RJ, Wilson RB, et al. 2005. AERMOD: A dispersion model for industrial source applications. Part I: General model formulation and boundary layer characterization. J Appl Meteor 44:682–693.

D'Onofrio D. 2015. Atlanta roadside emissions exposure study. Available: *https://atlantaregional.org/atlanta-roadside-emissions-exposure-study-arees/* [Accessed: June 2016].

Fujita EM, Campbell DE, Zielinska B, Chow JC, Lindhjem CE, DenBleyker A, et al. 2012. Comparison of the MOVES2010a, MOBILE6.2, and EMFAC2007 mobile source emission models with on-road traffic tunnel and remote sensing measurements. J Air Waste Manage Assoc 62:1134–1149.

Gordon TD, Tkacik DS, Presto AA, Zhang M, Jathar SH, Nguyen NT, et al. 2013. Primary gas- and particle-phase emissions and secondary organic aerosol production from gasoline and diesel off-road engines. Environ Sci Tech 47:14137–14146.

Heist D, Isakov V, Perry S, Snyder M, Venkatram A, Hood C, et al. 2013. Estimating near-road pollutant dispersion: A model inter-comparison. Transport Res Part D-Transport Environ 25:93-105.

Henneman LRF, Holmes HA, Mulholland JA, Russell AG. 2015. Meteorological detrending of primary and secondary pollutant concentrations: Method application and evaluation using long-term (2000-2012) data in Atlanta. Atmos Environ 119:201–210.

Hidy GM, Blanchard CL, Baumann K, Edgerton E, Tanenbaum S, Shaw S, et al. 2014. Chemical climatology of the southeastern United States, 1999-2013. Atmos Chem Phys 14:11893–11914.

Isakov V, Arunachalam S, Batterman S, Bereznicki S, Burke J, Dionisio K, Garcia V, Heist D, Perry S, Snyder M, Vette A. Air quality modeling in support of the near-road exposures and effects of urban air pollutants study (NEXUS). International journal of environmental research and public health. 2014 Aug 27;11(9):8777-93.

May AA, Nguyen NT, Presto AA, Gordon TD, Lipsky EM, Karve M, et al. 2014. Gas- and particle-phase primary emissions from in-use, on-road gasoline and diesel vehicles. Atmos Environ 88:247–260.

May AA, Presto AA, Hennigan CJ, Nguyen NT, Gordon TD, Robinson AL. 2013a. Gas-particle partitioning of primary organic aerosol emissions: (1) gasoline vehicle exhaust. Atmos Environ 77:128–139.

May AA, Presto AA, Hennigan CJ, Nguyen NT, Gordon TD, Robinson AL. 2013b. Gas-particle partitioning of primary organic aerosol emissions: (2) diesel vehicles. Environ Sci Tech 47:8288–8296.

Perry SG, Cimorelli AJ, Paine RJ, Brode RW, Weil JC, Venkatram A, et al. 2005. AERMOD: A dispersion model for industrial source applications. Part II: Model performance against 17 field study databases. J Appl Meteor 44:694–708.

Qian WJ, Venkatram A. 2011. Performance of steady-state dispersion models under low wind-speed conditions. Boundary-Layer Meteor 138:475–491.

Ranjan M, Presto AA, May AA, Robinson AL. 2012. Temperature dependence of gas-particle partitioning of primary organic aerosol emissions from a small diesel engine. Aerosol Sci Tech 46:13–21.

Snyder MG, Venkatram A, Heist DK, Perry SG, Petersen WB, Isakov V. 2013. RLINE: A line source dispersion model for near-surface releases. Atmos Environ 77:748–756.

Stelson AW, Seinfeld JH. 1982. Relative-humidity and temperature-dependence of the ammonium-nitrate dissociation-constant. Atmos Environ 16:983–992.

Tkacik DS, Lambe AT, Jathar S, Li X, Presto AA, Zhao YL, et al. 2014. Secondary organic aerosol formation from in-use motor vehicle emissions using a potential aerosol mass reactor. Environ Sci Tech 48:11235–11242.

U.S. Environmental Protection Agency. 2000. Meteorological monitoring guidance for regulatory modeling applications.

U.S. Environmental Protection Agency. 2004. User's guide for the aermod meteorological preprocessor (AERMET).

U.S. Environmental Protection Agency. 2014. Motor Vehicle Emission Simulator (MOVES). Available: *www.epa.gov/otaq/models/moves/* [accessed 15 August 2017].

U.S. Environmental Protection Agency. 2015. Aerminute user's guide. Available: *https://www3.epa.gov/ttn/scram/7thconf/aermod/aerminute_userguide.pdf*

Venkatram A, Isakov V, Pankratz D, Heumann J, Yuan J. 2004. The analysis of data from an urban dispersion experiment. Atmos Environ 38:3647–3659.

Venkatram A, Schulte N. 2014. On formulating equations for plume spreads for near-surface releases. Int J Environ Pollut 54:156–165.

Venkatram A, Snyder M, Isakov V. 2013a. Modeling the impact of roadway emissions in light wind, stable and transition conditions. Transport Res Part D-Transport Environ 24:110–119.

Venkatram A, Snyder MG, Heist DK, Perry SG, Petersen WB, Isakov V. 2013b. Re-formulation of plume spread for near-surface dispersion. Atmos Environ 77:846–855.

Watson JG, Chow JC, Lowenthal DH, Chen LWA, Shaw S, Edgerton ES, et al. 2015. PM2.5 source apportionment with organic markers in the Southeastern Aerosol Research and Characterization (SEARCH) study. J Air Waste Manage Assoc 65:1104–1118.

Zhai X, Russell AG, Sampath P, Mulholland JA, Kim BU, Kim Y, D'Onofrio D. Calibrating R-LINE model results with observational data to develop annual mobile source air pollutant fields at fine spatial resolution: Application in Atlanta. Atmospheric Environment. 2016 Dec 31;147:446–57.

Zhao YL, Nguyen NT, Presto AA, Hennigan CJ, May AA, Robinson AL. 2015. Intermediate volatility organic compound emissions from on-road diesel vehicles: Chemical composition, emission factors, and estimated secondary organic aerosol production. Environ Sci Tech 49:11516–11526.

Zhao YL, Nguyen NT, Presto AA, Hennigan CJ, May AA, Robinson AL. 2016. Intermediate volatility organic compound emissions from on-road gasoline vehicles and small off-road gasoline engines. Environ Sci Tech 50:4554–4563.

Appendix E: Personal Exposures — Matching by Sampling Week

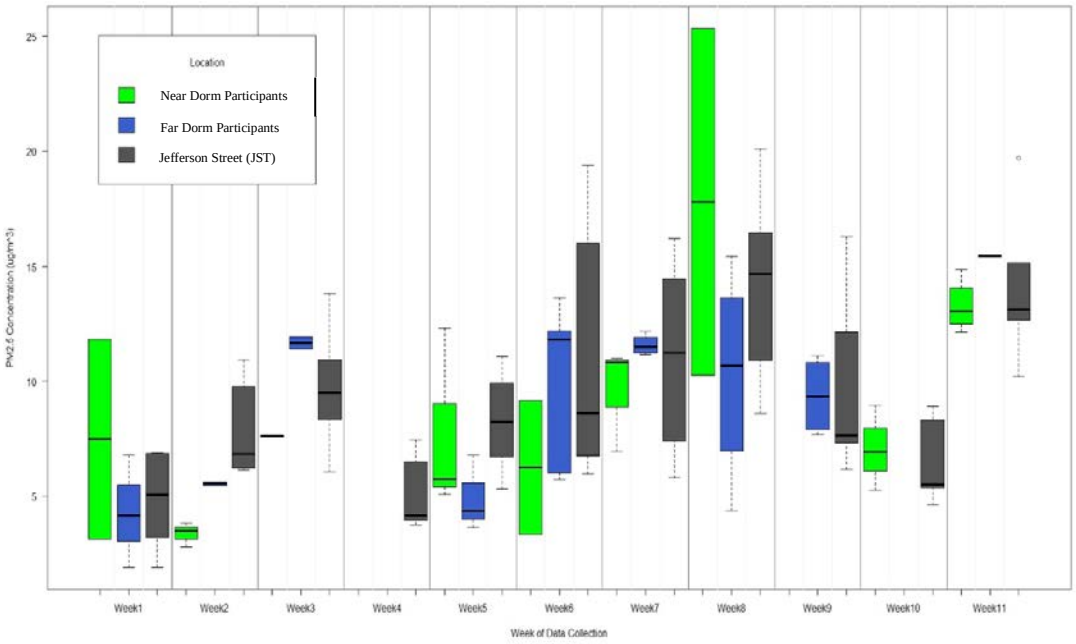

Figure E.1. Weekly distribution of personal $PM_{2.5}$ exposures by participant dorm residence and corresponding ambient $PM_{2.5}$ concentration in ($\mu g/m^3$) at the JST site.

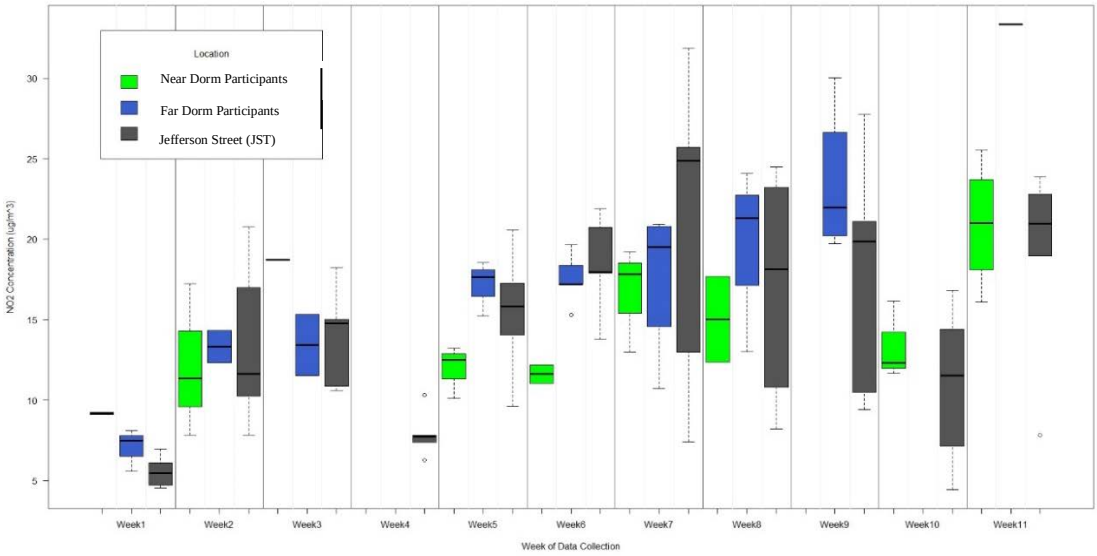

Figure E.2. Weekly distribution of personal NO_2 exposures by participant dorm residence and corresponding ambient NO_2 concentration (ppb) at the JST site.

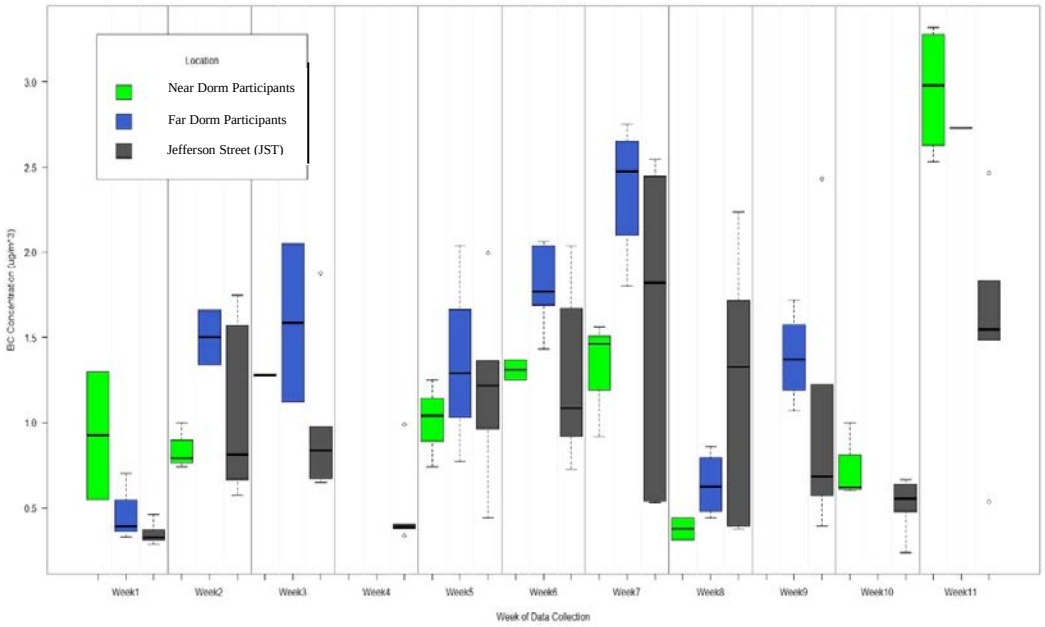

Figure E.3. Weekly distribution of personal BC exposures by participant dorm residence and corresponding ambient BC concentration ($\mu g/m^3$) **at the JST site.**

Appendix F: Metabolomics Analysis

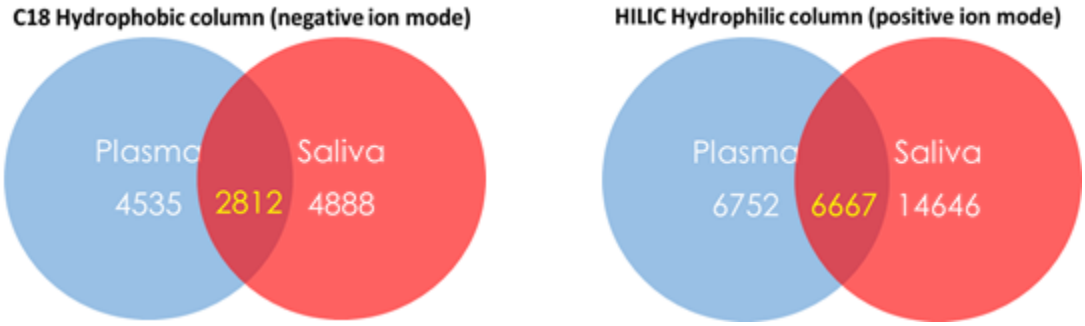

Figure F.1. **Shared features between plasma and saliva samples.** In the C18 column, 7,347 metabolites were extracted in each plasma sample and 7,700 in each saliva sample, with 2,812 common features shared by both plasma and saliva samples. In the HILIC column, 13,419 metabolites were extracted in each plasma sample and 21,313 in each saliva sample, with 6,667 common features shared by both plasma and saliva samples.